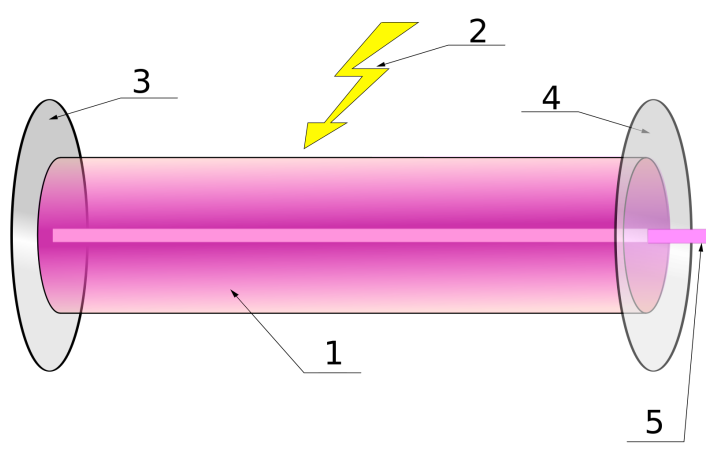
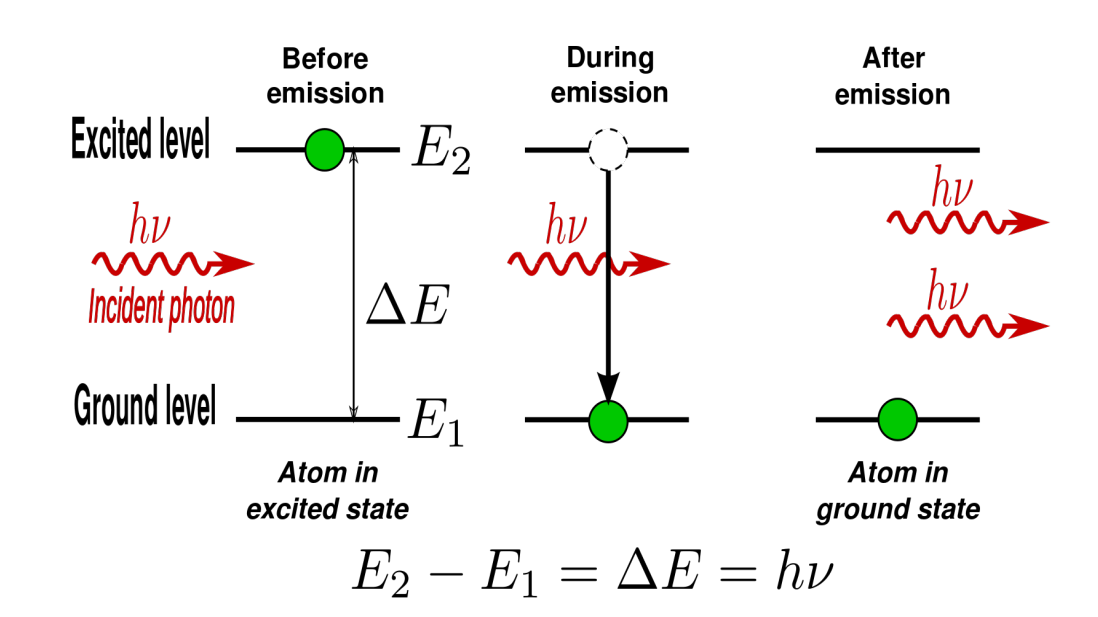
Laser

The term "laser" originated as an acronym for "light amplification by stimulated emission of radiation".



- 1. Gain medium
- 2. Laser pumping energy
- 3. High reflector
- 4. Output coupler
- 5. Laser beam



Types of Lasers

Lasers are commonly designated by the type of lasing material employed, which can be a solid, gas, liquid or semiconductor.

Solid-state lasers have lasing material distributed in a solid matrix (such as the ruby or neodymium:yttrium-aluminum garnet "Yag" lasers). The neodymium-Yag laser emits infrared light at 1,064 nm.

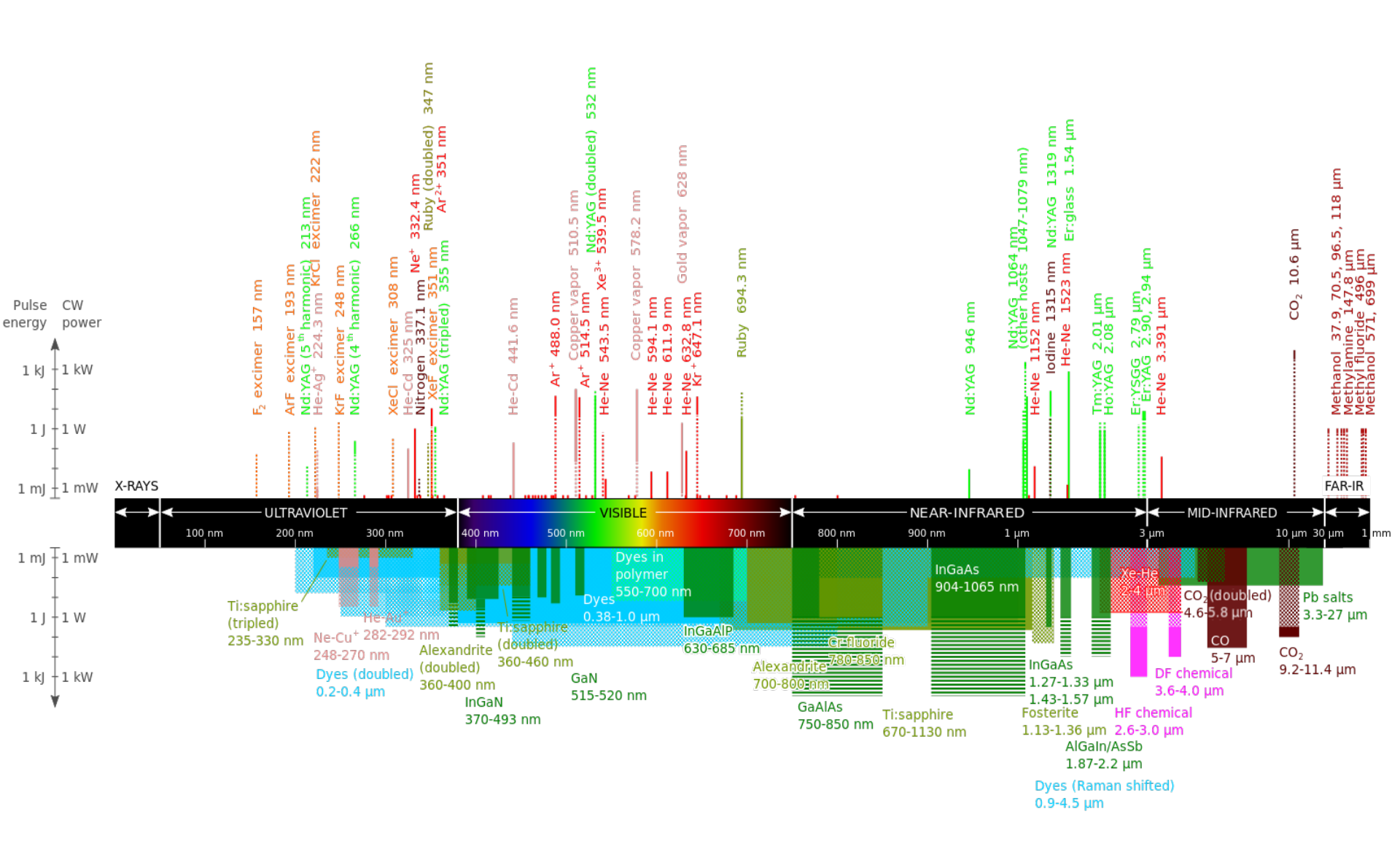
Gas lasers (helium and helium-neon, HeNe, are the most common gas lasers) have a primary output of visible red light. CO₂ lasers emit energy in the far-infrared, and are used for cutting hard materials.

Excimer lasers use reactive gases, such as chlorine and fluorine, mixed with inert gases such as argon, krypton or xenon. When electrically stimulated, a pseudo molecule (dimer) is produced. When lased, the dimer produces light in the ultraviolet range.

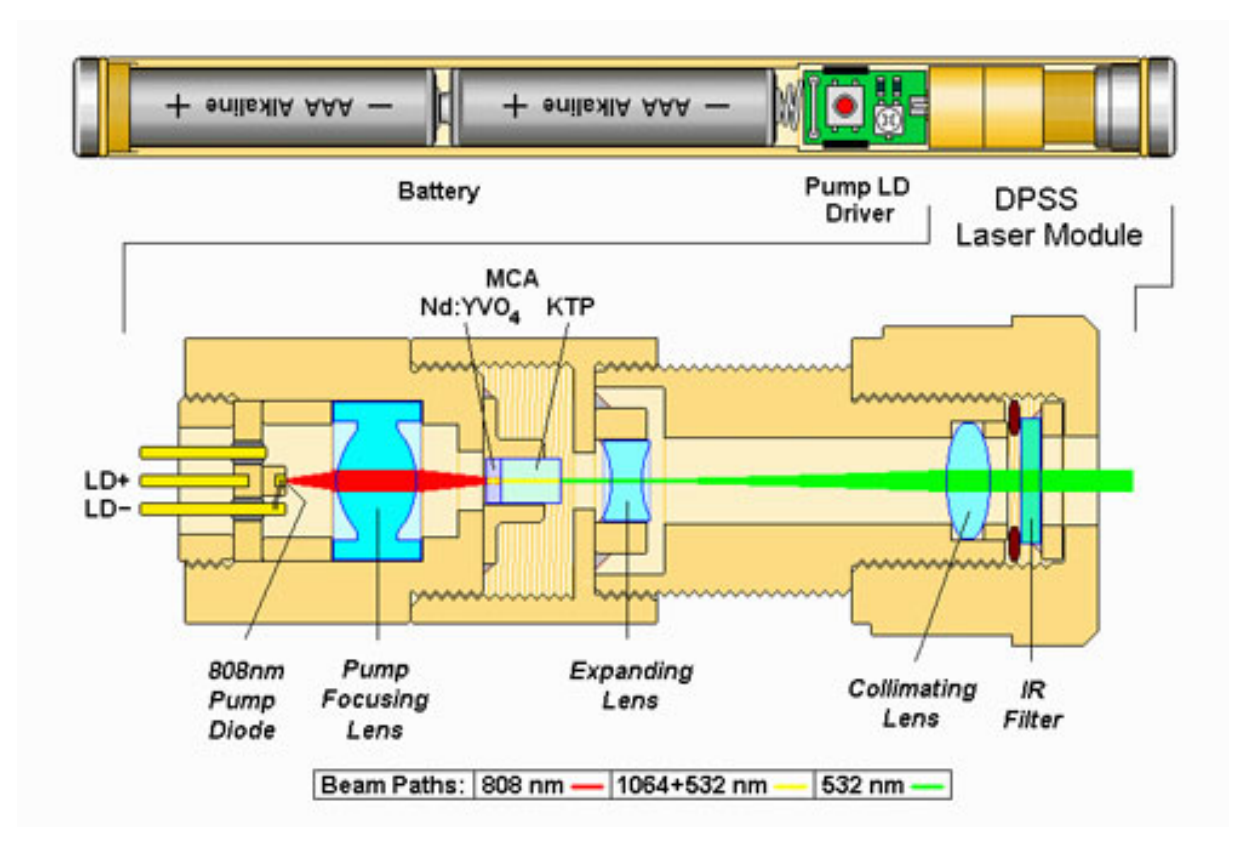
Dye lasers use complex organic dyes, such as rhodamine 6G, in liquid solution or suspension as lasing media. They are tunable over a broad range of wavelengths.

Semiconductor lasers, sometimes called diode lasers, are not solid-state lasers. These electronic devices are generally very small and use low power. They may be built into larger arrays, such as the writing source in some laser ² printers or CD players.

Wavelengths of commercially available lasers



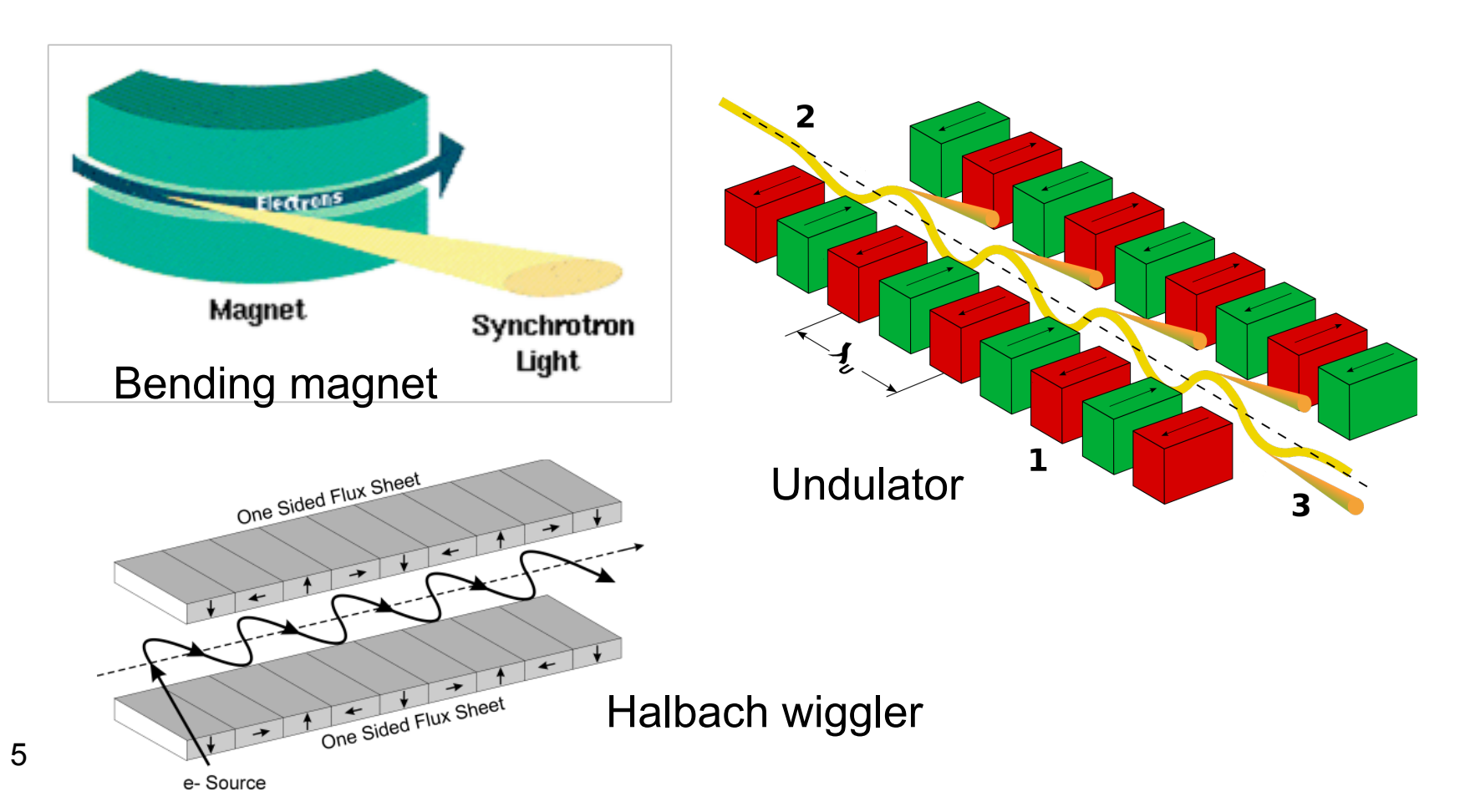
Frequency-doubled green laser pointer



Two AAA cells and electronics power the laser module, which contains a powerful 808 nm IR diode laser that optically pumps a $Nd:YVO_4$ crystal inside a laser cavity. That laser produces 1064 nm (infrared) light which is mainly confined inside the resonator. Also inside the laser cavity, however, is a non-linear KTP crystal which causes frequency doubling, resulting in green light at 532 nm. The front mirror is transparent to this visible wavelength which is then expanded and collimated using two lenses.

Synchrotron Radiation

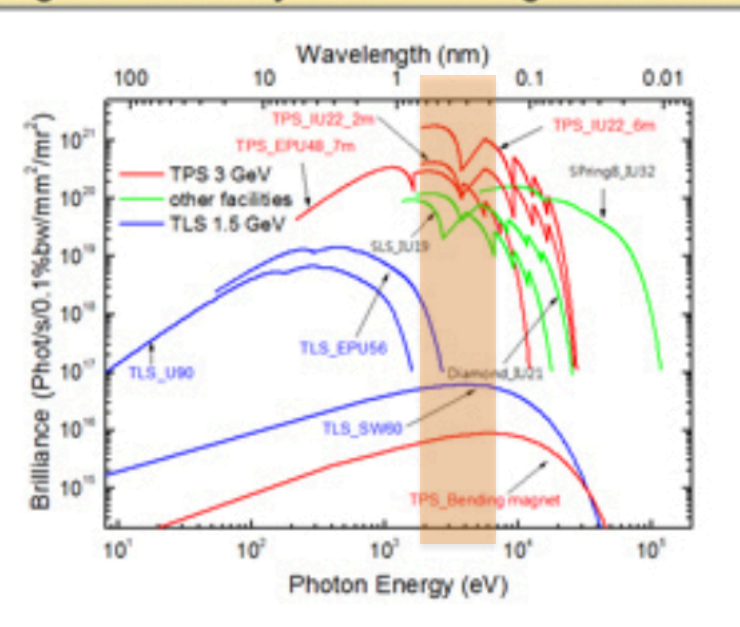
The electromagnetic radiation emitted when charged particles are accelerated radially is called **synchrotron radiation**. The radiation produced in this way has a characteristic polarization and the frequencies generated can range over the entire electromagnetic spectrum.



Synchrotron Radiation

Taiwan Photon Source (TPS)

Brightness of Synchrotron Light Sources



Parameters of TPS Synchrotron Facility

Energy	3 GeV
Beam Current	500 mA at 3 GeV
C of the Storage Ring	518.4 m (h = 864)
C of the Booster	496.8 m (h = 828)
Cells	24-cell DBA
Straight Sections	12 m x 6 (σ_{V} = 9.8 μ m, σ_{h} = 165.1 μ m) 7 m x 18 (σ_{V} = 5.1 μ m, σ_{h} = 120.8 μ m)
mittance	1.6 nm·rad at 3 GeV (Distributed dispersion)
RF frequency	499.654 MHz
Critical Energy	7.13 keV (dipole)
Energy Loss/turn	853 keV (dipole)

The light source and its experimental facilities will be open to the academic and scientific communities to conduct advanced research in 2014.

Spectroscopy at nanometer scale

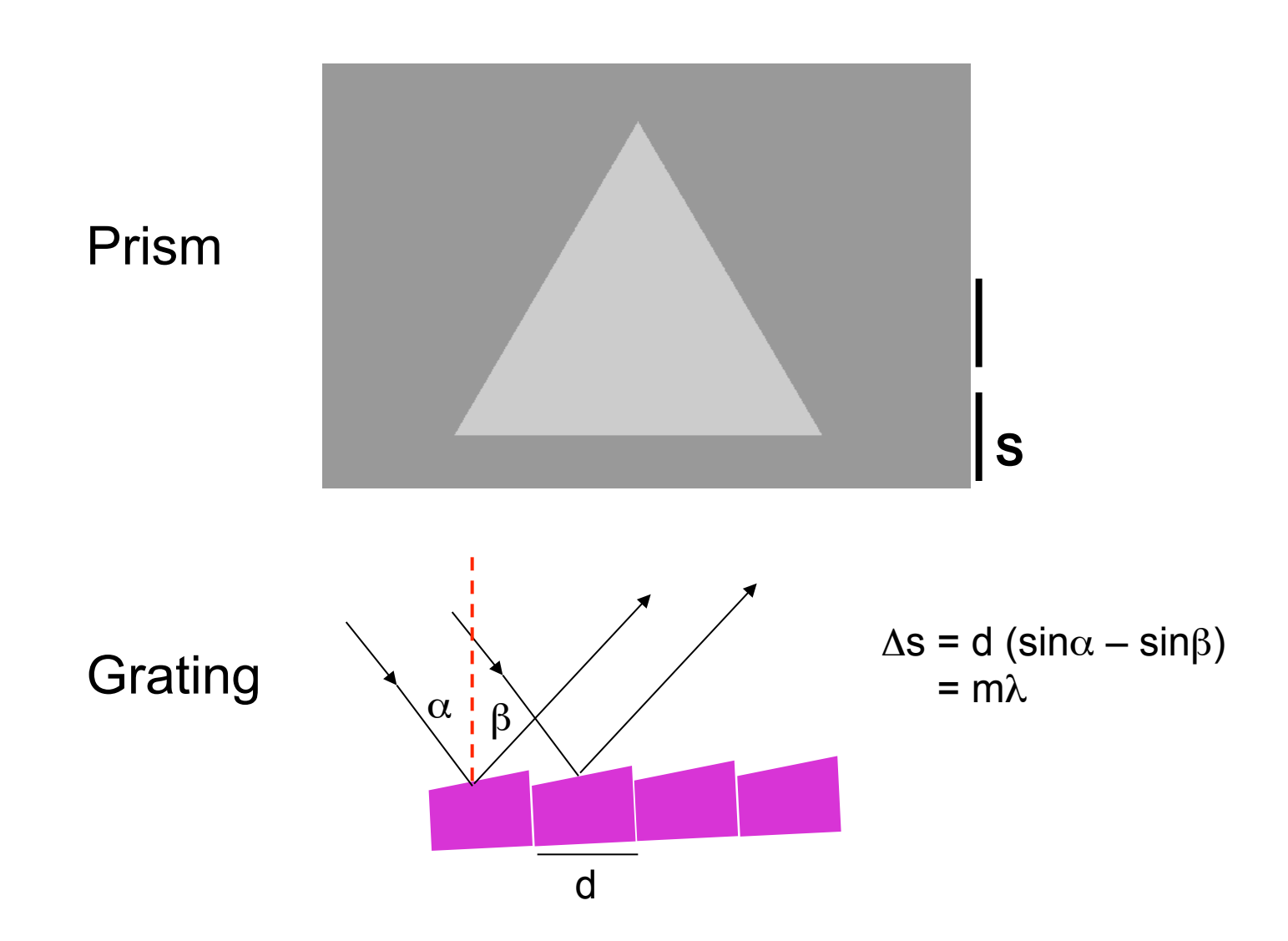
- 1. Spectroscopy vs. Microscopy
- 2. Spectroscopies for H and H₂
- 3. Physics and Chemistry of nanomaterials

Microscopy is the science of investigating small objects that are too small for the naked eye. The microscopic study involves revelation of the structure and morphology of the matter under investigation.

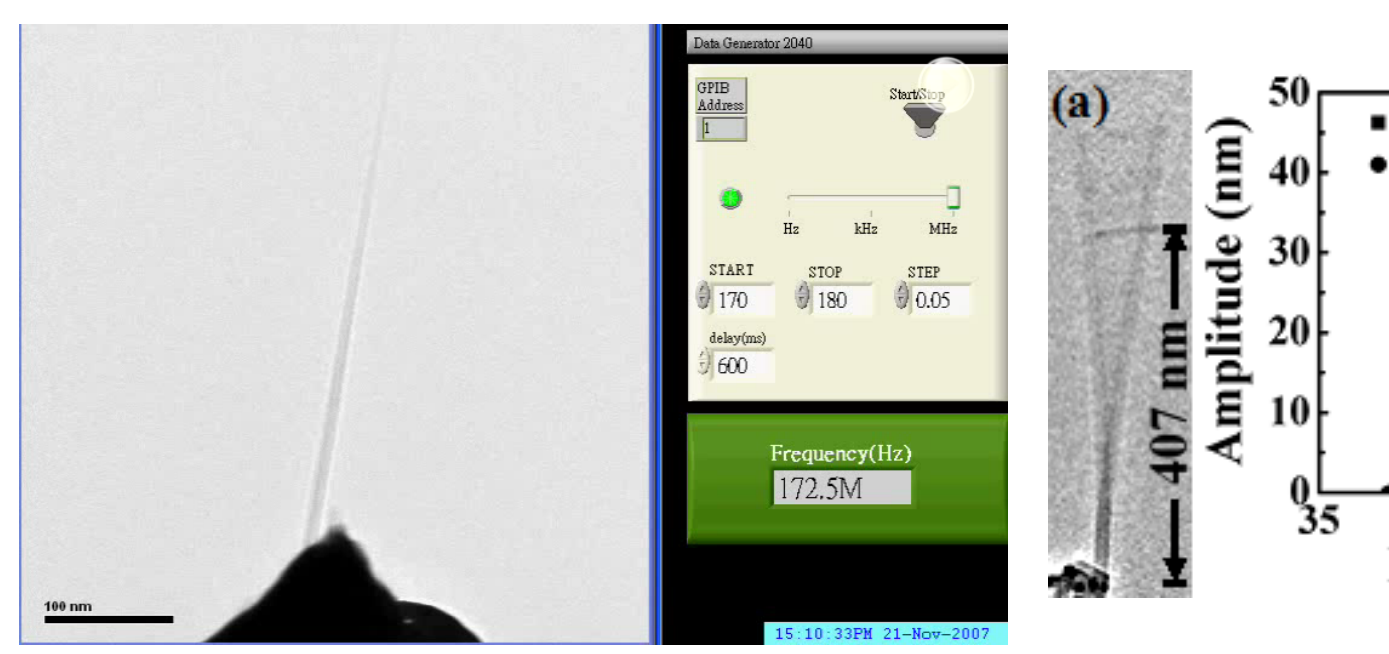
Spectroscopy is the study of the interaction between matter and radiated energy. With the mechanism of "resonance", the characteristic nature of the matter can be probed.

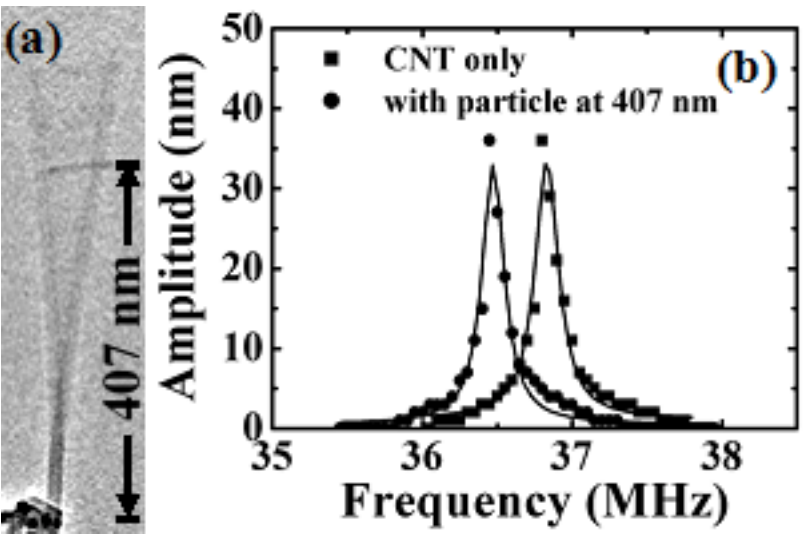
Both microscopic and spectroscopic techniques are essential for nanoscience research.

Spectroscopy originates from the dispersion of light through a prism.



Mechanical resonance

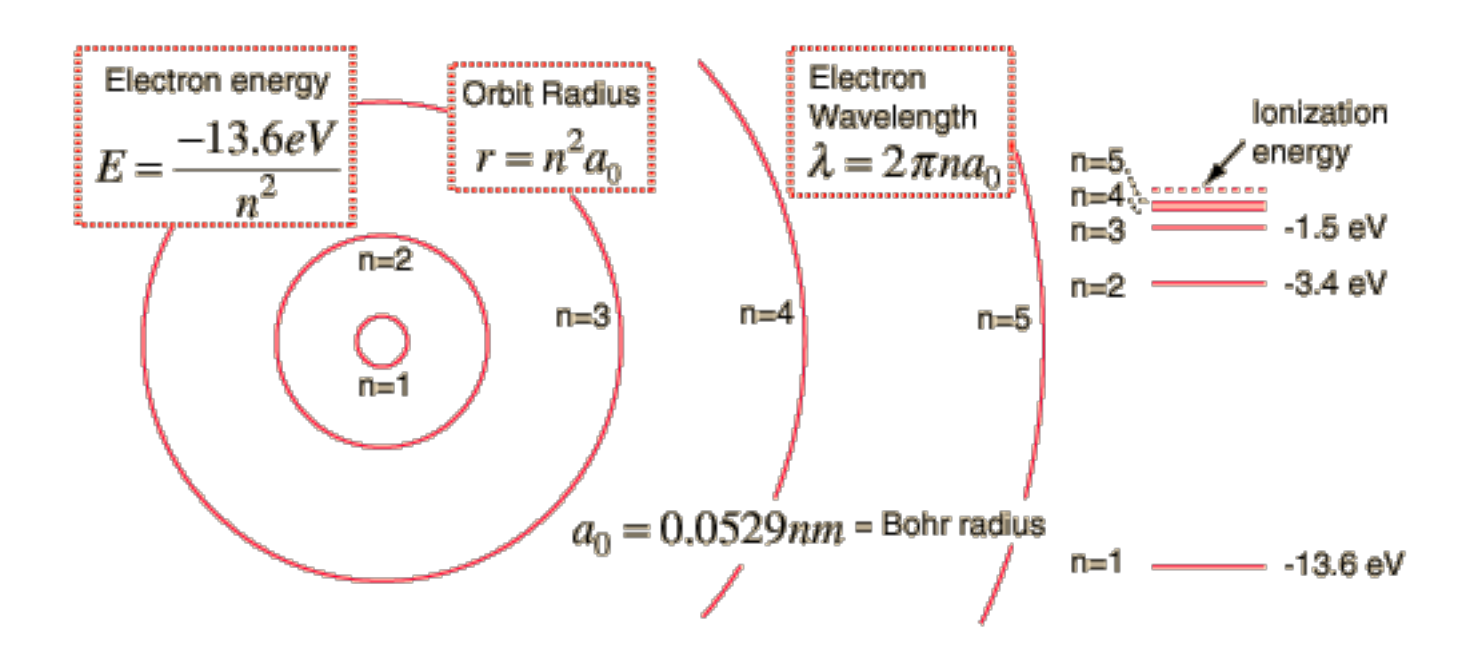




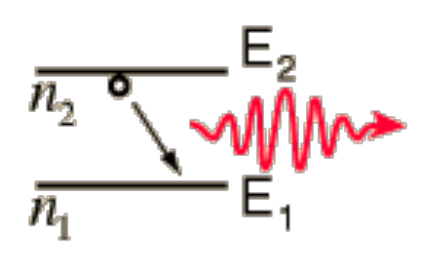
Bohr model of hydrogen atom

$$E = -\frac{Z^{2}me^{4}}{8n^{2}h^{2}\varepsilon_{0}^{2}} = \frac{-13.6Z^{2}}{n^{2}}eV \qquad r = \frac{n^{2}h^{2}\varepsilon_{0}}{Z\pi me^{2}} = \frac{n^{2}a_{0}}{Z}$$

$$a_{0} = 0.0529nm = Bohr \ radius$$



Electron Transitions



A downward transition involves emission of a photon of energy:

a photon of energy:
$$\mathsf{E}_{\mathsf{photon}} = h\upsilon = \mathsf{E}_2 - \mathsf{E}_1$$

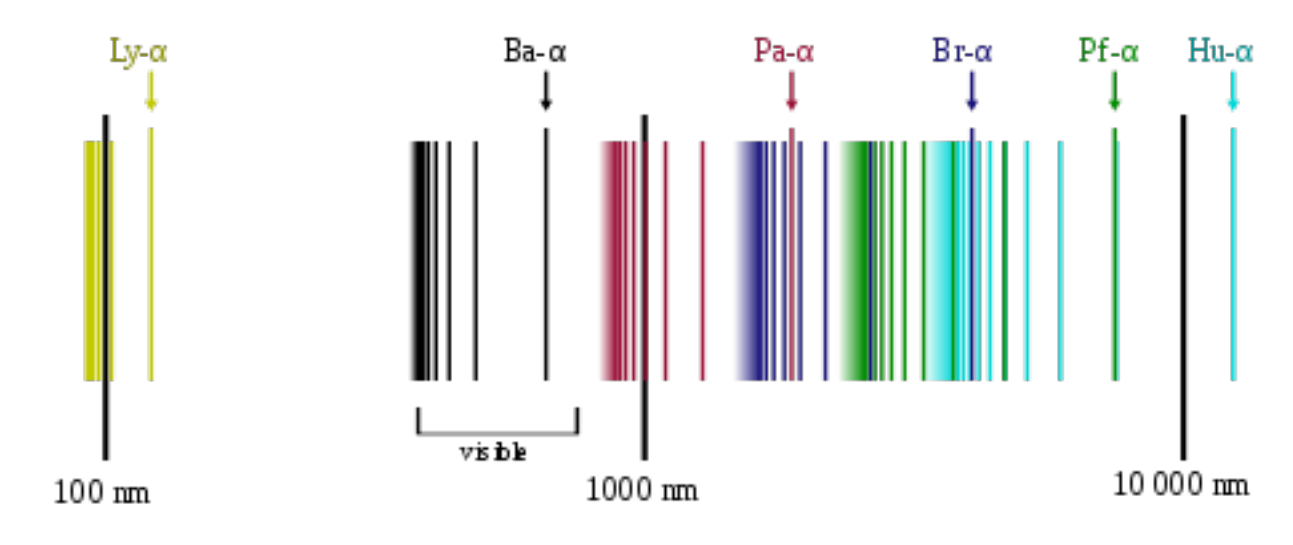
Given the expression for the energies of the hydrogen electron states:

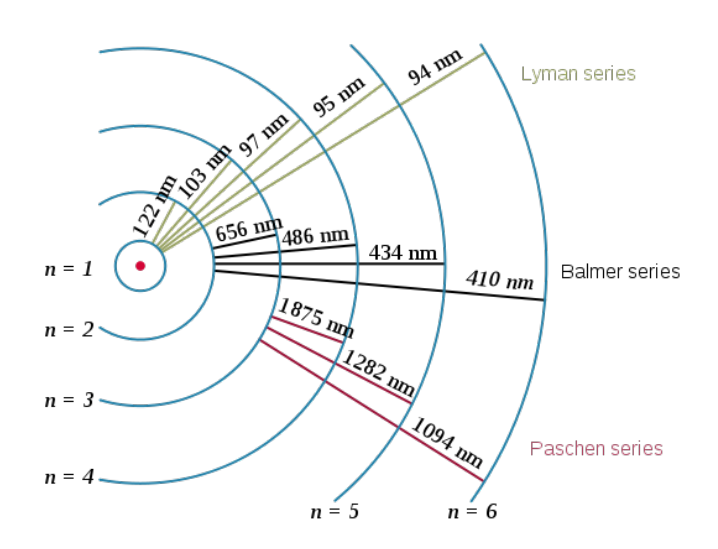
$$hv = \frac{2\pi^2 me^4}{h^2} \left[\frac{1}{n_1^2} - \frac{1}{n_2^2} \right] = -13.6 \left[\frac{1}{n_1^2} - \frac{1}{n_2^2} \right] \text{eV}$$

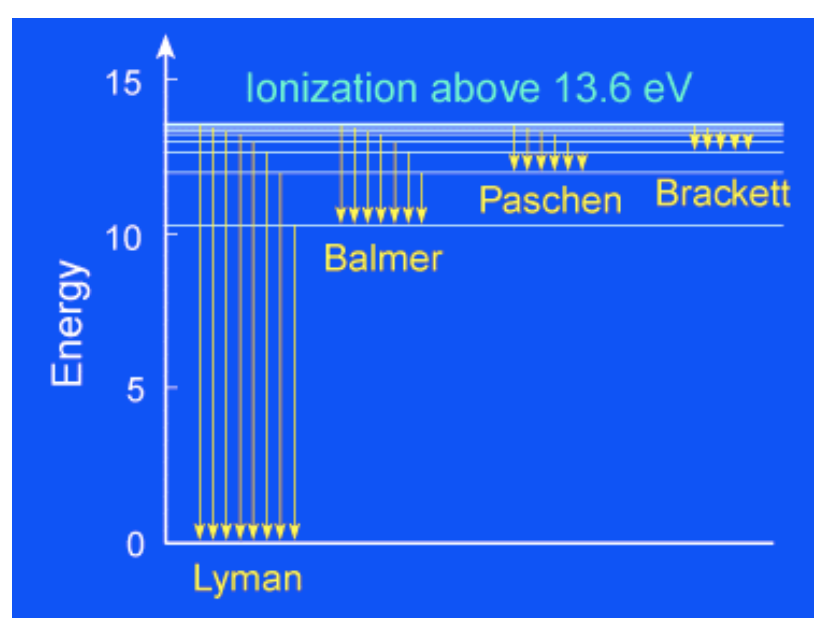
Fermi's golden rule is a way to calculate the transition rate (probability of transition per unit time) between two eigenstates

$$T_{i\to f} = \frac{2\pi}{\hbar} \left| \langle f|H'|i\rangle \right|^2 \rho,$$

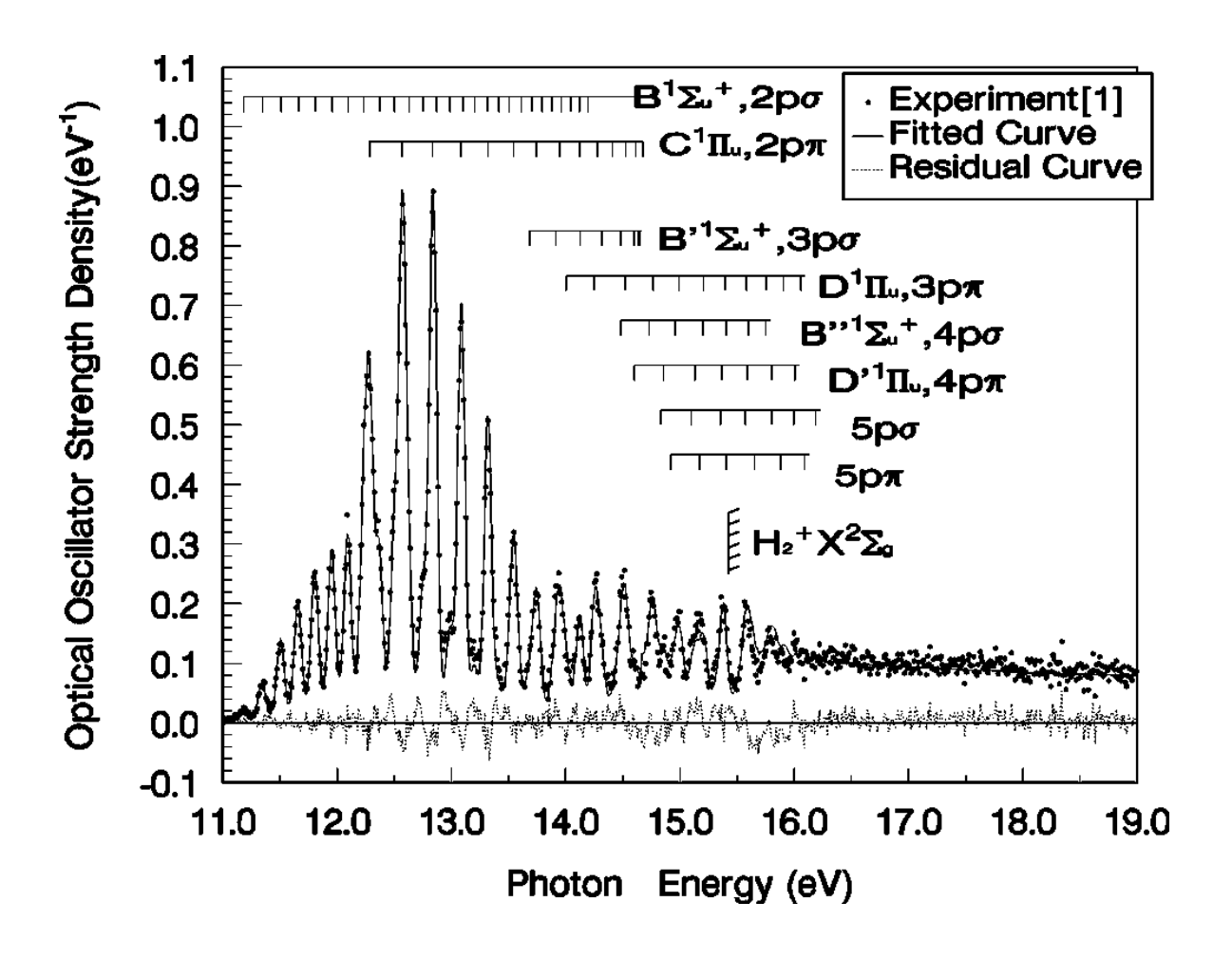
Absorption spectra of atomic hydrogen





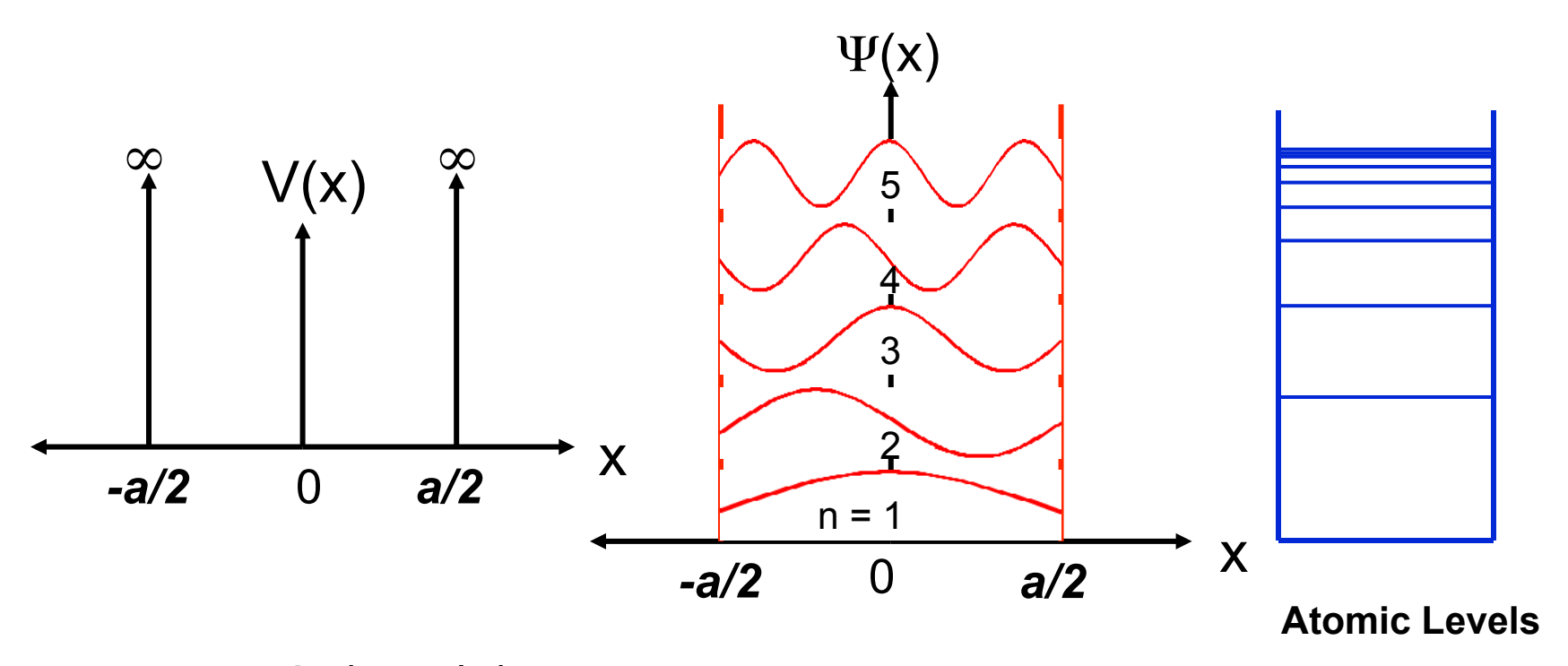


Absorption spectra of molecular hydrogen



Zhi Ping Zhong et al., Phys. Rev. A **60**, 236 (1999)

One dimensional size effect

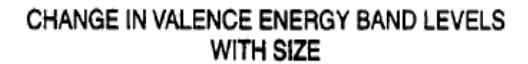


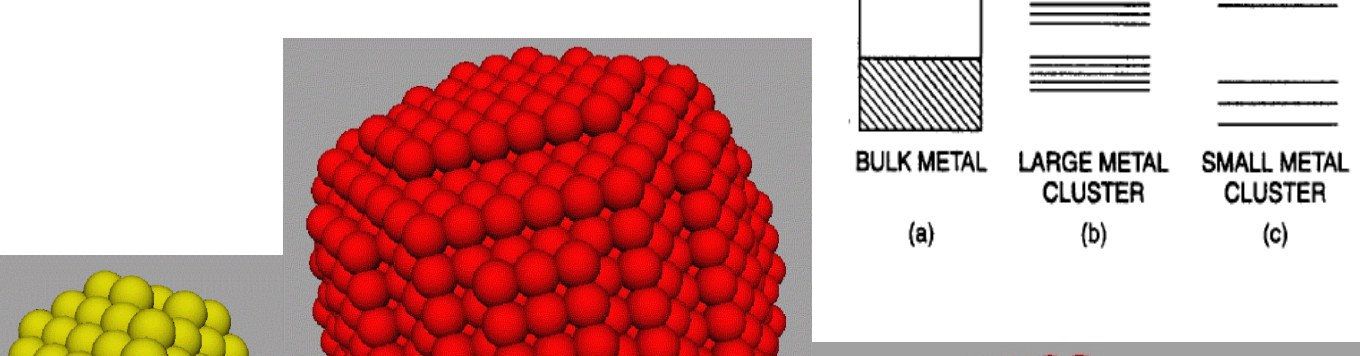
$$\Psi(x) = \begin{cases} \sin(n\pi x/a), & n \text{ even} \\ \cos(n\pi x/a), & n \text{ odd} \end{cases}$$

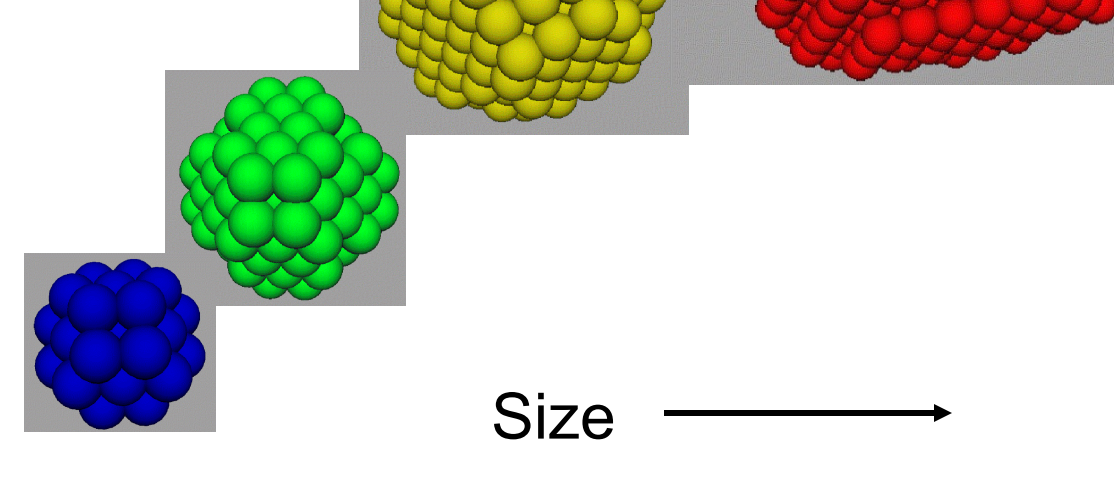
$$E = n^2 \pi^2 \hbar^2 / 2ma^2$$
, $n = 1, 2, 3...$

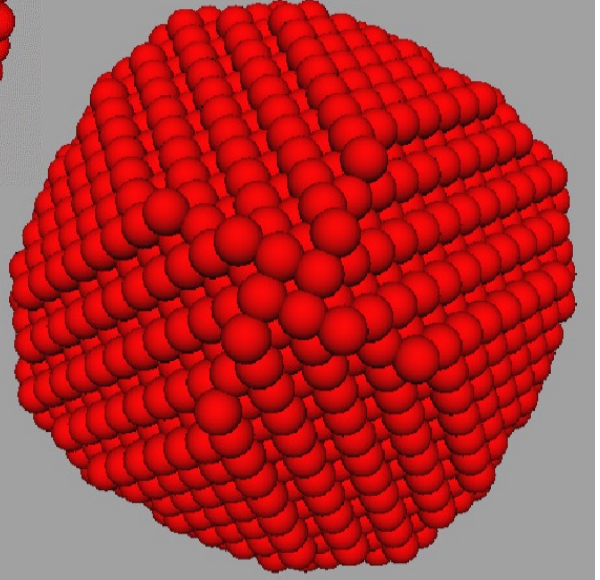


Size effect

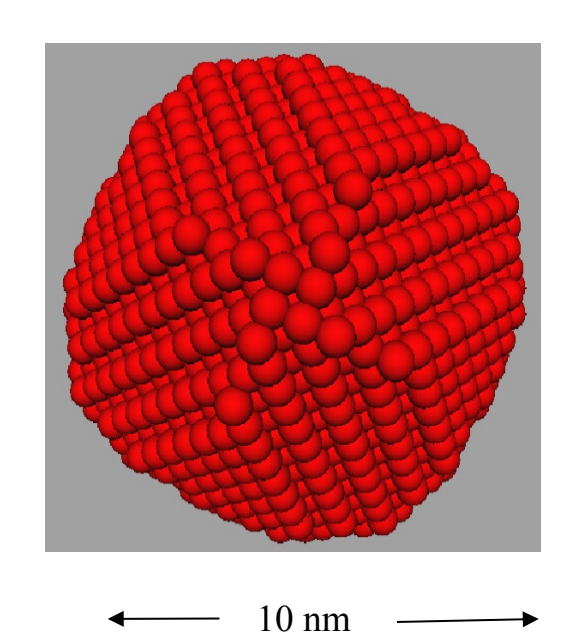








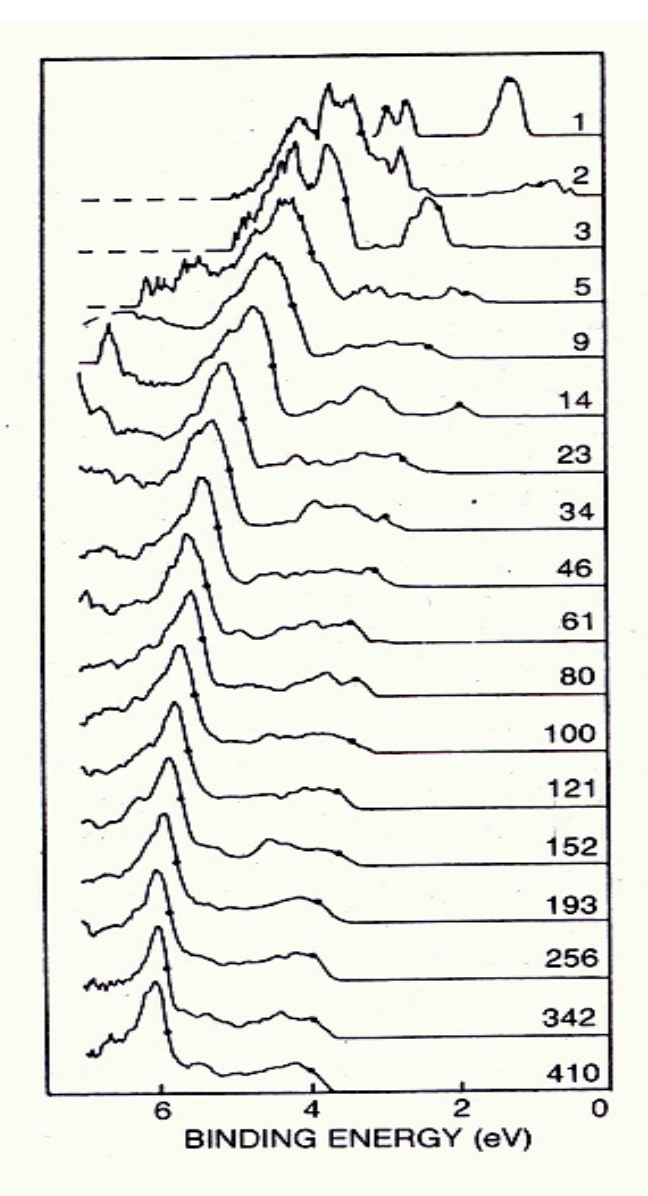
Au nanoparticle as an example



$$E_F = (\hbar^2/2m) (3\pi^2 n)^{2/3}$$
 $g(E_F) = (3/2) (n/E_F)$
 $\delta = 2/[g(E_F)V] = (4/3) (E_F/N)$

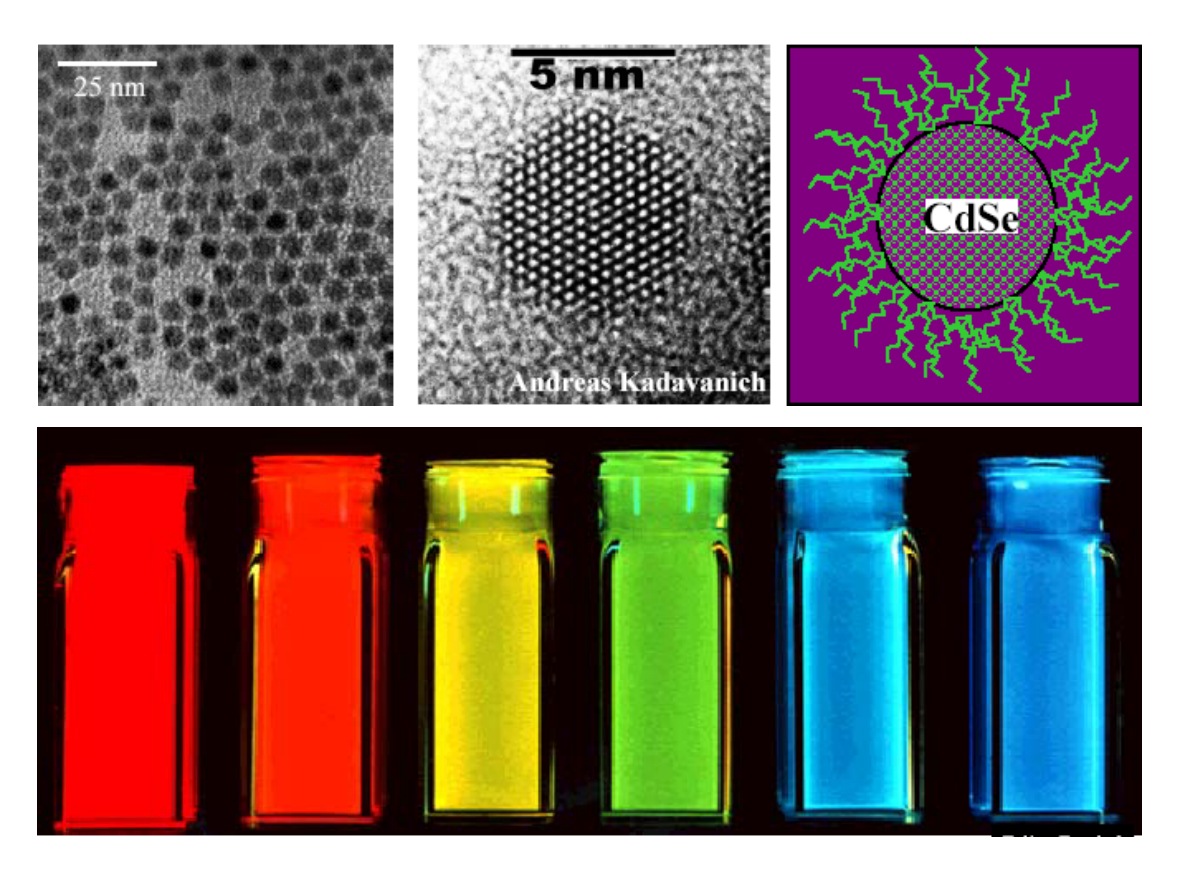
Number of valence electrons (N) contained in the particles is roughly 40,000. Assume the Fermi energy ($E_{\rm F}$) is about 7 eV for Au, then

 $\delta \sim 0.22 \text{ meV} \sim 2.5 \text{ K}$

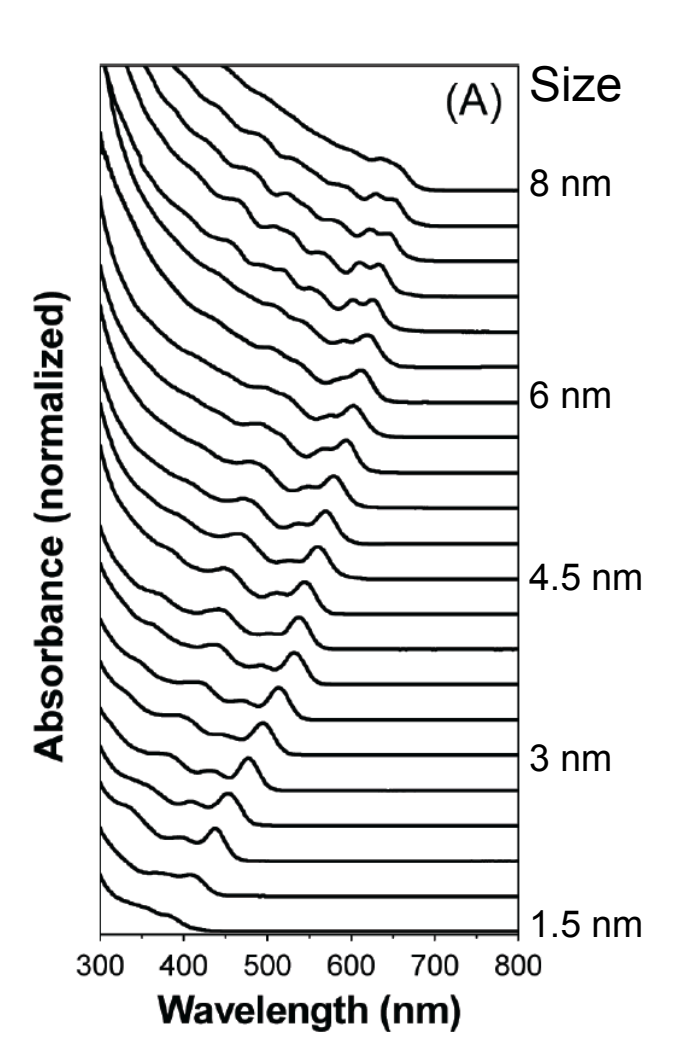


Ultraviolet photoemission spectra of ionized copper clusters Cu, ranging in size from N of 1 to 410 show the energy distribution versus binding energy of photoemitted electrons. These photoemission patterns show the evolution of the 3d band of Cu as a function of cluster size. As the cluster size increases, the electron affinity approaches the value of the bulk metal work function. (Adapted from ref. 10.) Figure 5

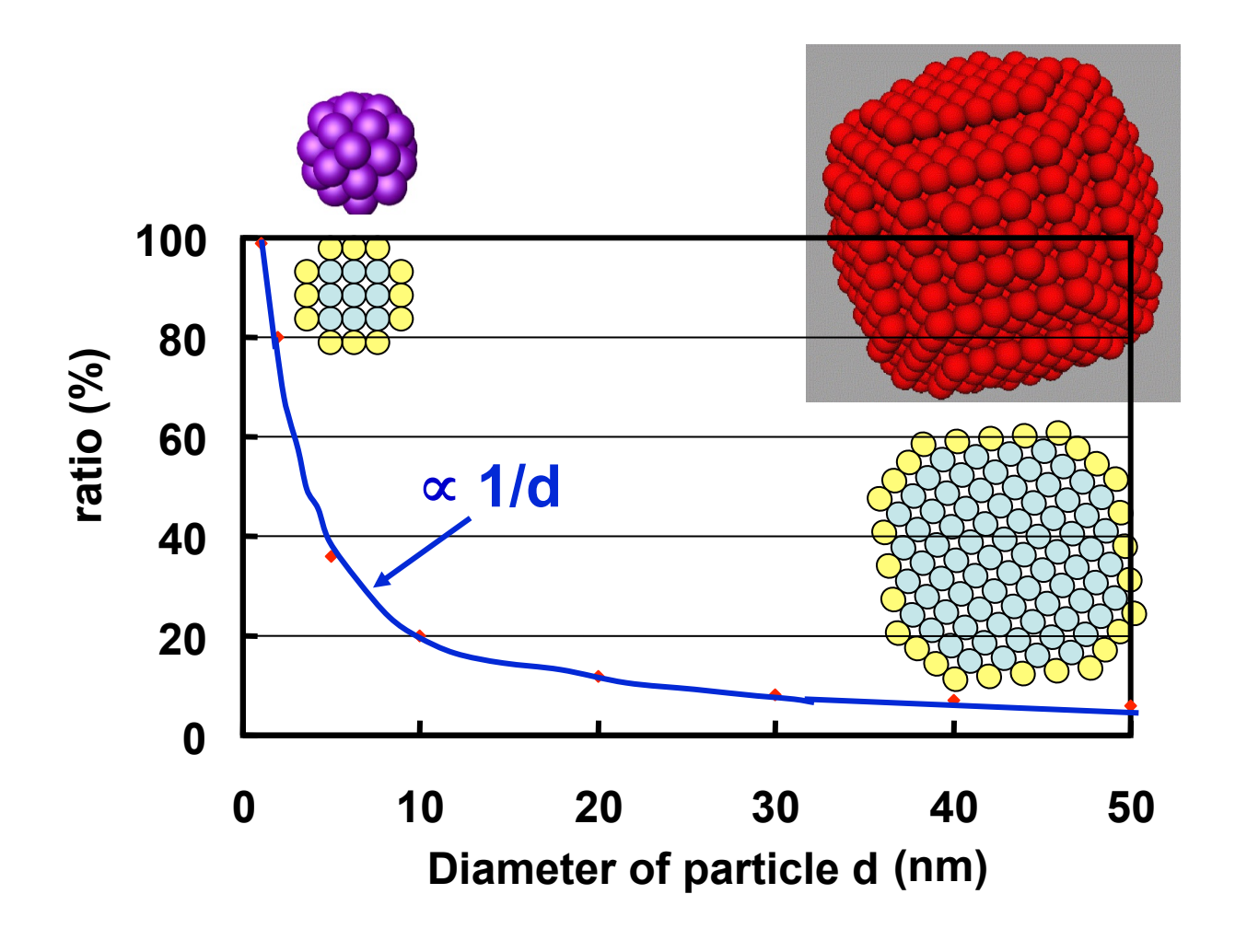
Semiconductor quantum dots



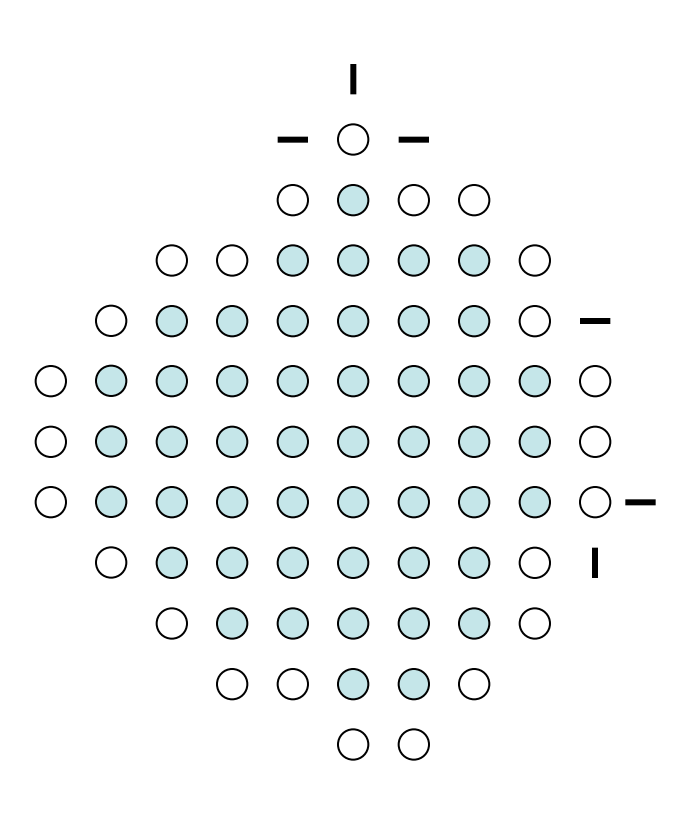
(Reproduced from Quantum Dot Co.)



Ratio of surface atoms



Optical properties of nanoparticles (in the infrared range)



- (1) Broad-band absorption: Due mainly to the increased normal modes at the surface.
- (2) Blue shift:

 Due mainly to the bond shortening resulted from surface tension or phonon confinement.

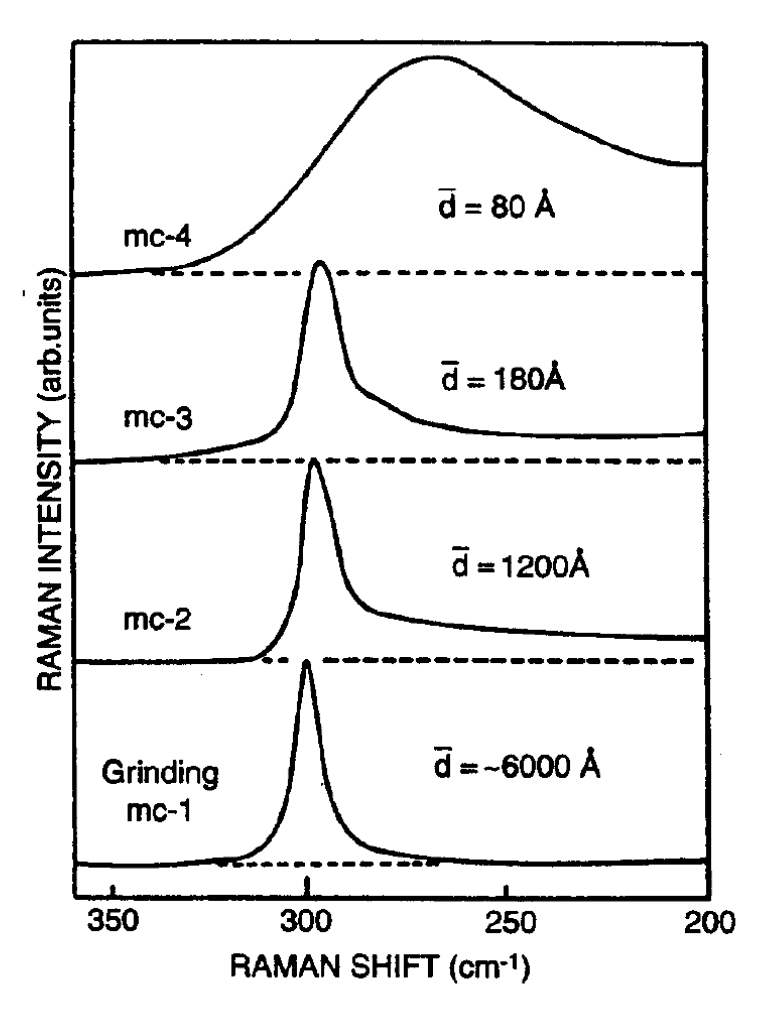


Figure 8.11. Raman spectra of Ge nanocrystallites produced by gas condensation showing the broadening and shift to lower wavenumbers as the particle size decreases. The lowest spectrum was obtained from ground bulk germanium. [From S. Hayashi, M. Ito, and H. Kanamori, *Solid State Commun.* **44**, 75 (1982).]

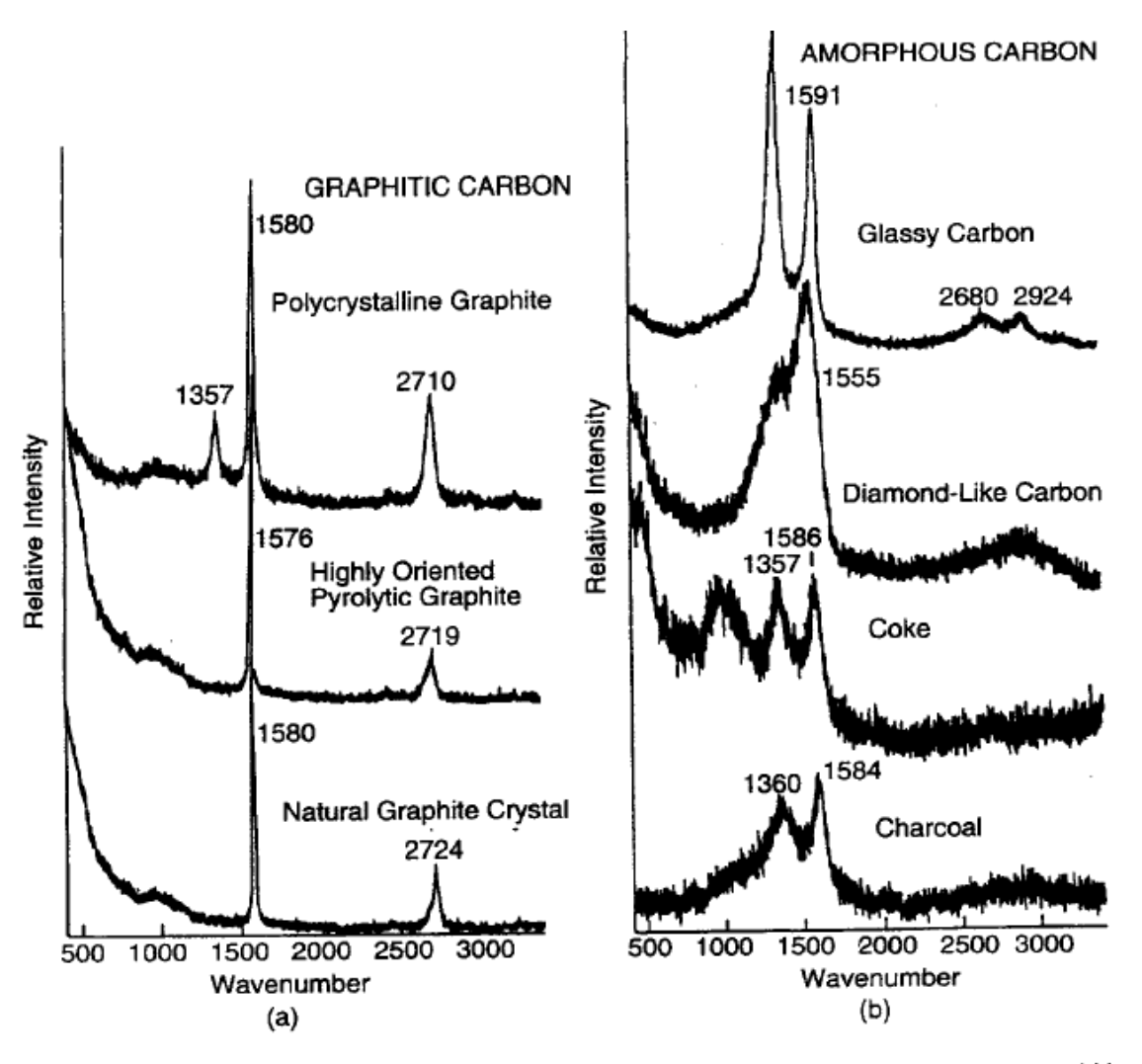
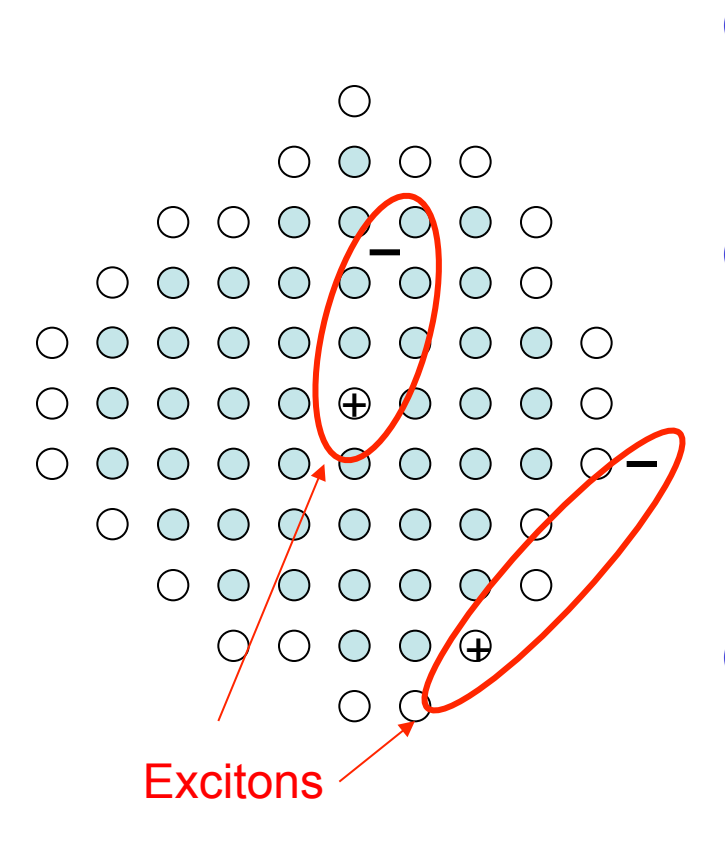


Figure 8.19. Raman spectra of (a) crystalline graphites and (b) noncrystalline, mainly graphitic, carbons. The *D* band appears near 1355 cm⁻¹ and the *G* band, near 1580 cm⁻¹. [From D. S. Knight and W. B. White, *J. Mater, Sci.* **4**, 385 (1989).]

Optical properties of nanoparticles (in the visible light range)



(1) Blue shift:

Due mainly to the energy-gap widening because of the size effect.

(2) Red shift:

Bond shortening resulted from surface tension causes more overlap between neighboring electron wavefunctions. Valence bands will be broadened and the gap becomes narrower.

(3) Enhanced exciton absorption: Due mainly to the increased probability of exciton formation because of the confining effect.

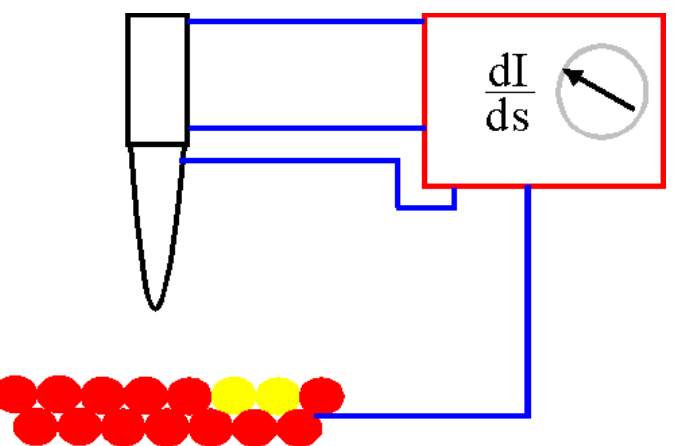
Scanning Tunneling Spectroscopy

1. Barrier Height Imaging

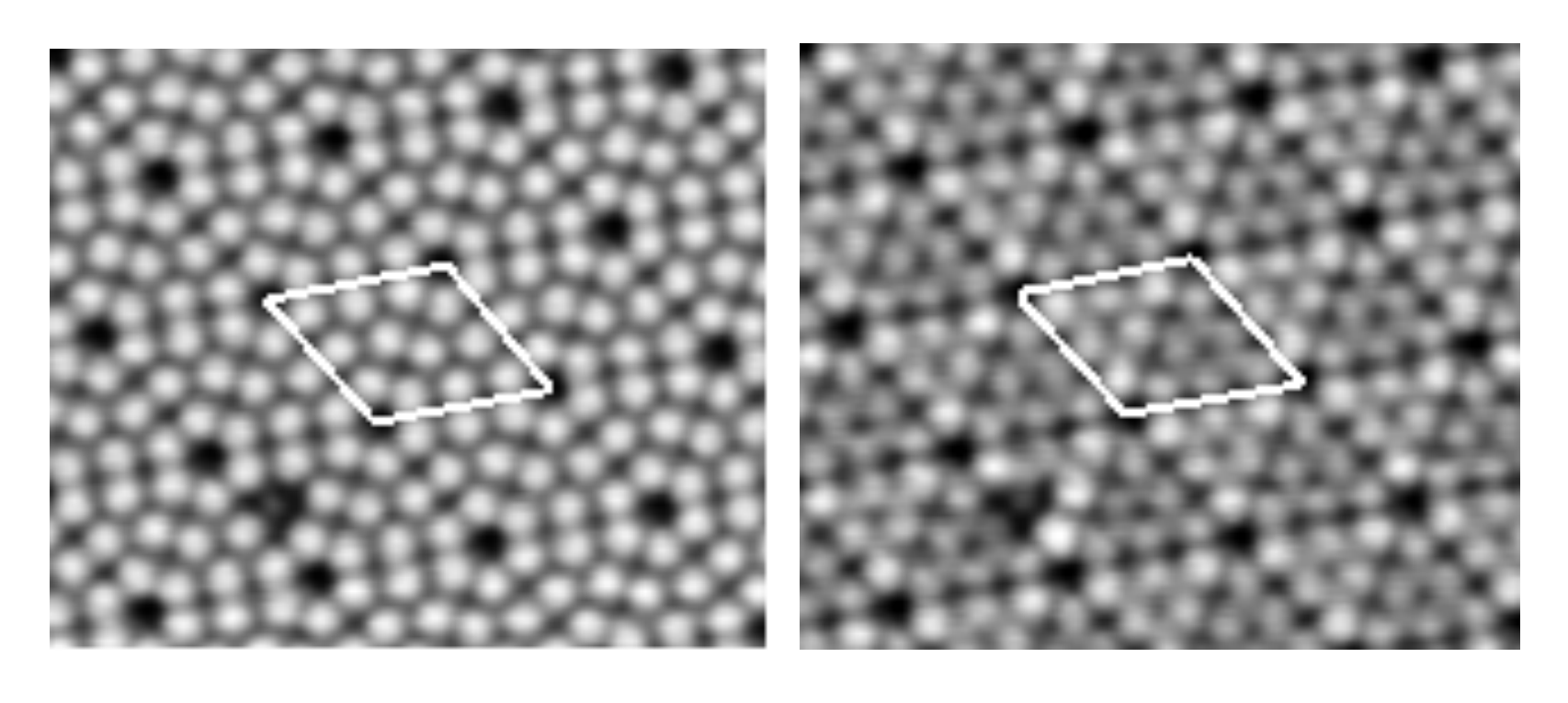
Up to now homogeneous surfaces were considered. If there is an inhomogeneous compound in the surface the work function will be inhomogeneous as well. This alters the local barrier height. Differentiation of tunneling current yields

$$rac{ ext{d}(\ln ext{I})}{ ext{ds}} \propto \sqrt{\Phi}$$

Thus the work function can directly be measured by varying the tip-sample distance, which can be done by modulating the current with the feedback turned on.



STM Images of Si(111)-(7×7)



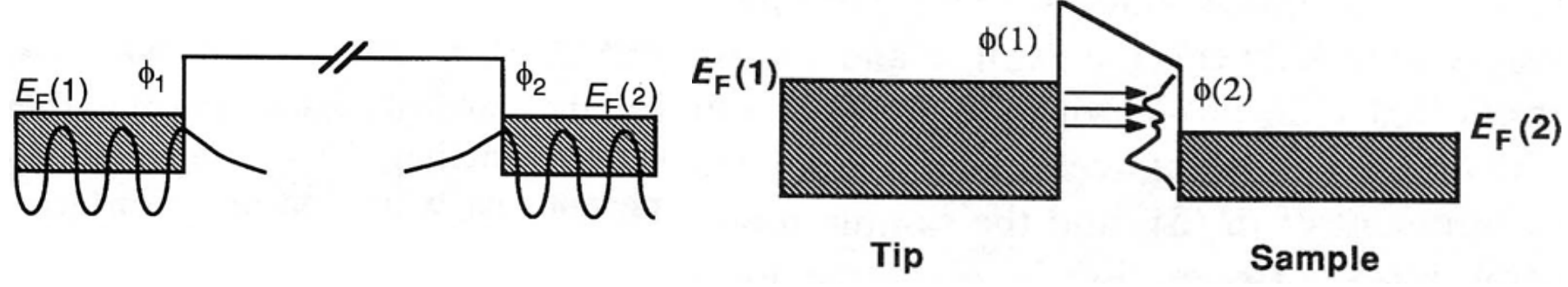
Empty-state image

Filled-state image

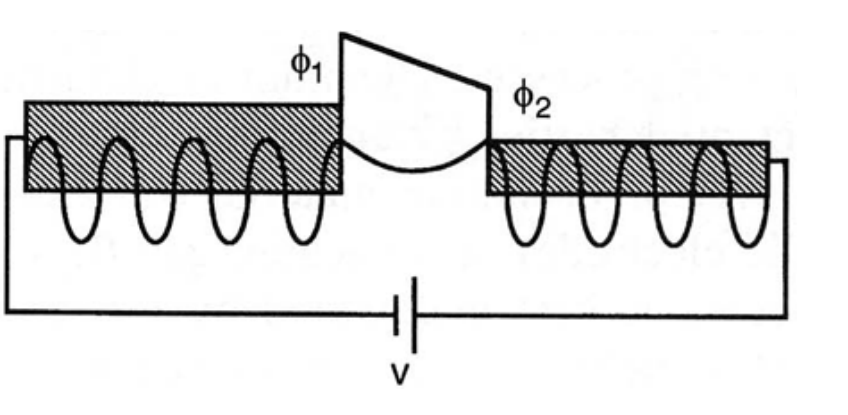
Electronic Structures at Surfaces

Empty-State Imaging

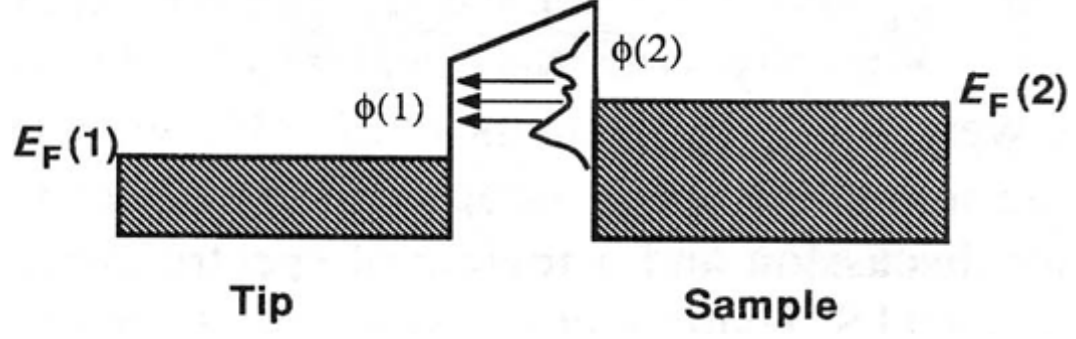




Tunneling



Filled-State Imaging



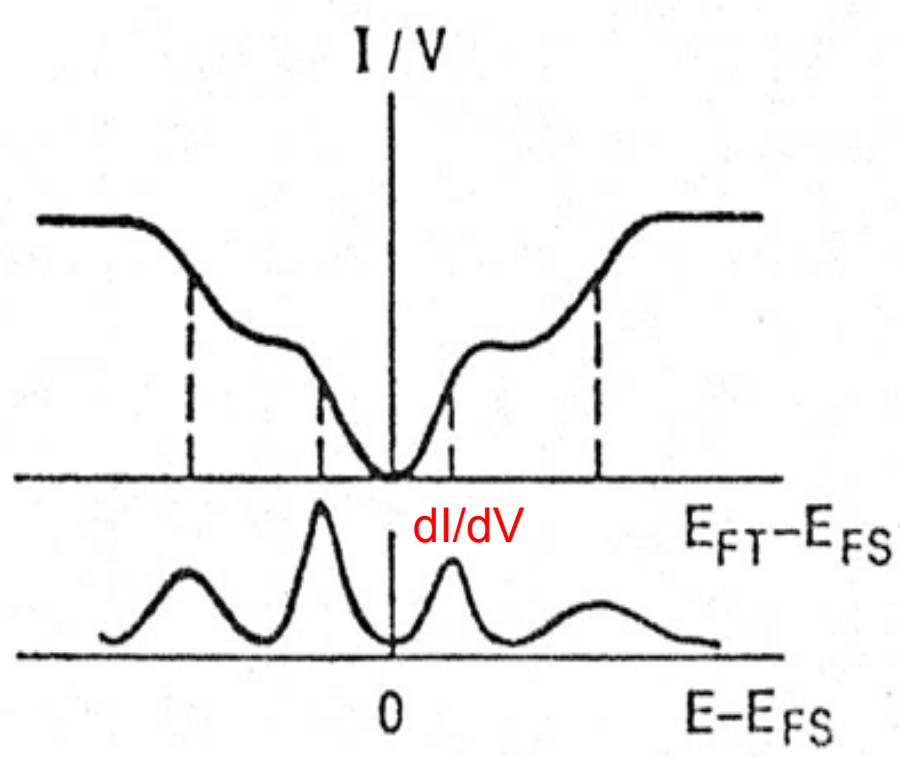
2. dl/dV imaging

If the matrix element and the density of states of the tip is nearly constant, the tunneling current can be estimated to

$$I \propto \int\limits_0 \rho_{\rm sa} \Big(E_F - eV + \epsilon \Big) d\epsilon$$

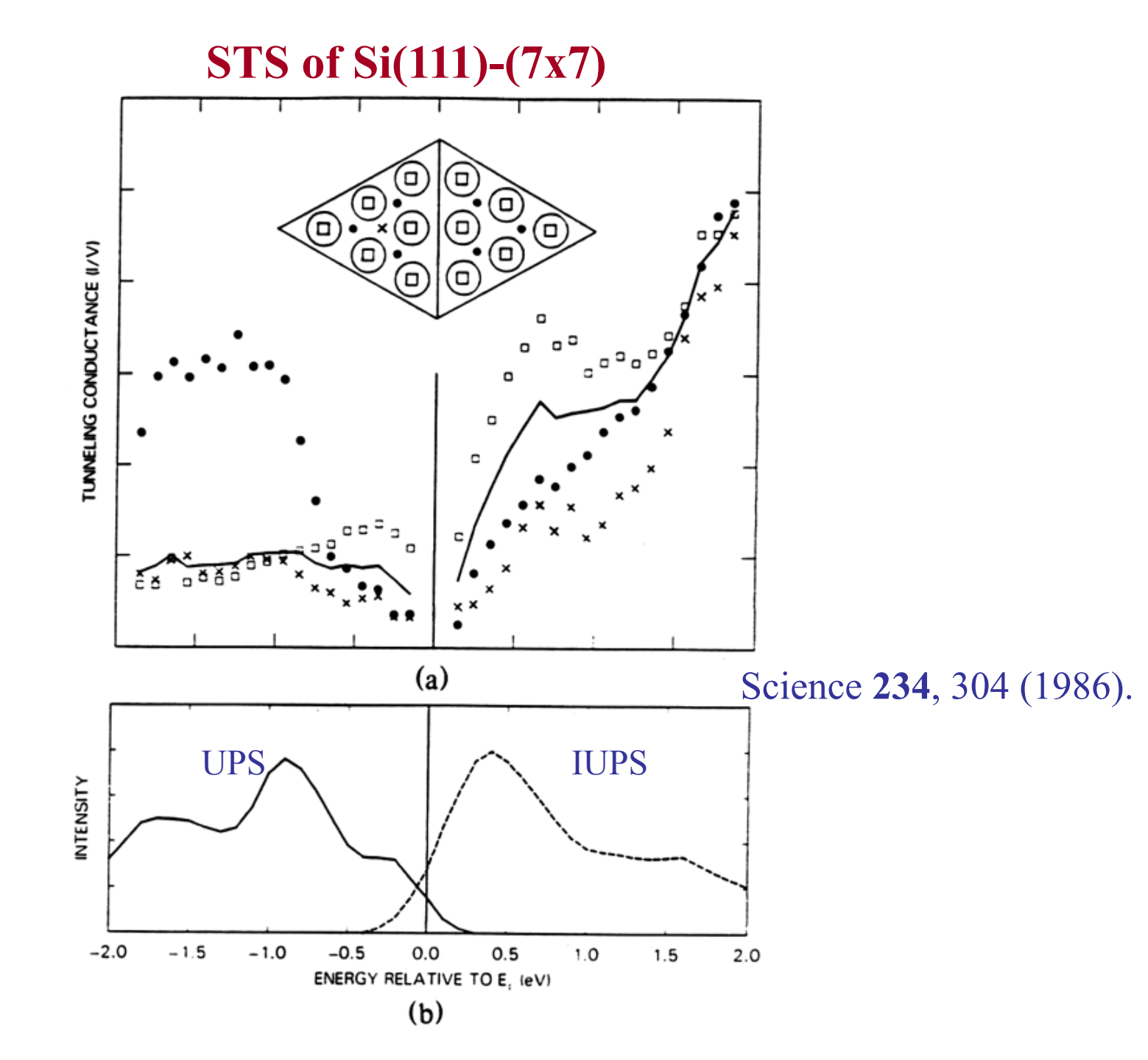
Differentiation yields the density of state:

$$\frac{dI}{dV} \propto \rho_{sa} \Big(E_F - eV \Big)$$



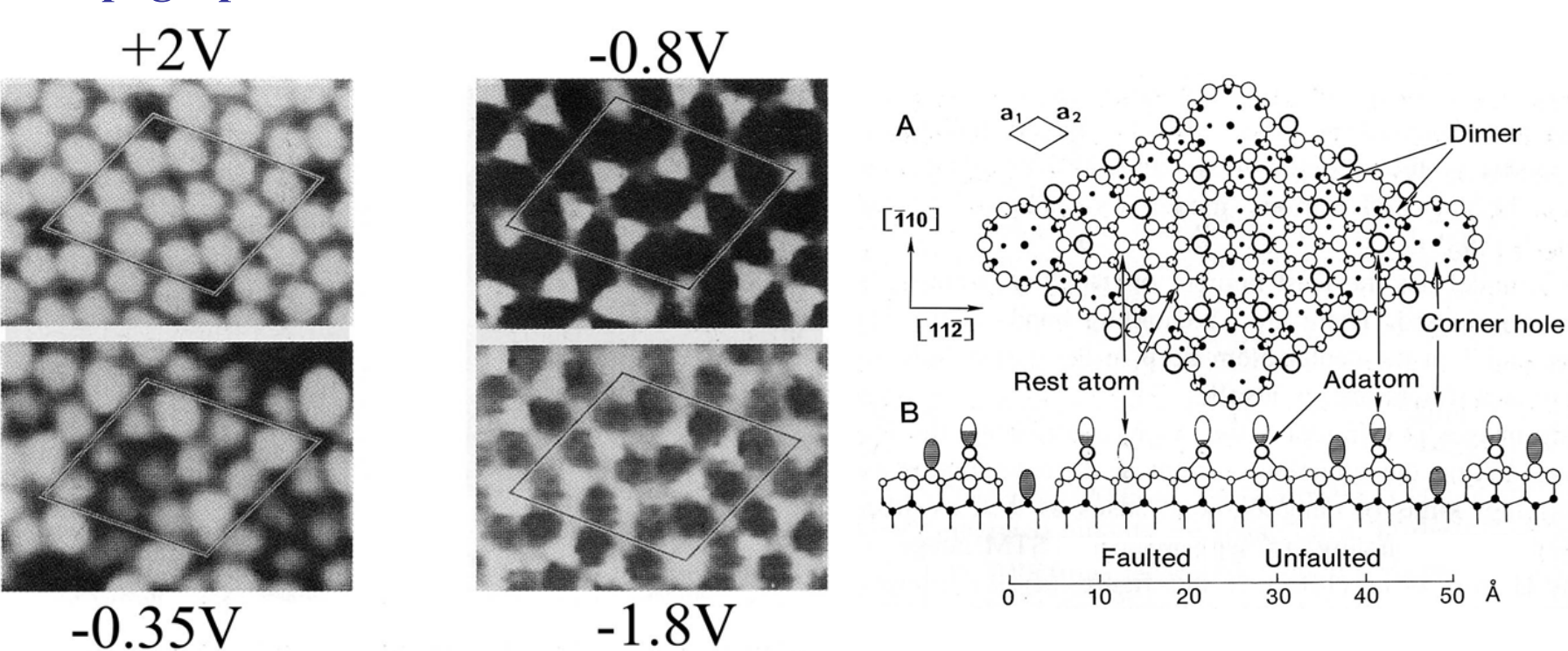
Density of state (DOS)

- The mapping of surface density of states can be deduced by
- Modulation of the bias voltage (dl/dV imaging):
 The tip is scanned in the constant current mode to give a constant distance to the sample. A dither voltage of ~1k Hz is added to the bias voltage while the feedback loop remains active. A lock-in technique is employed to obtain the current change at the dither frequency.
- Current-Imaging Tunneling Spectroscopy (CITS):
 The tip is scanned in the constant current mode to give a constant distance to the sample. At each point the feedback loop is disabled and a current-voltage curve (I-V curve) is recorded.



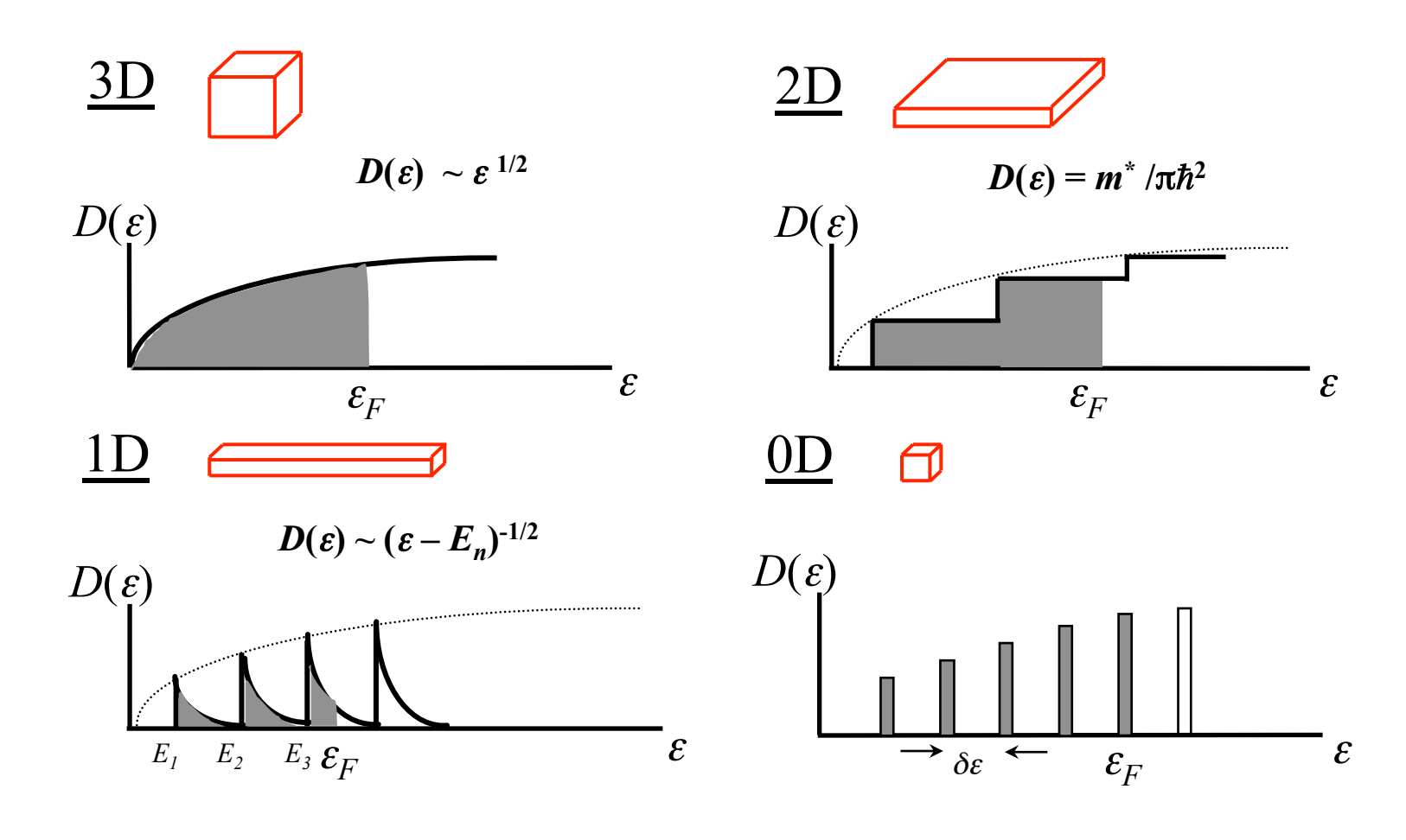
STS of Si(111)-(7x7)

topograph

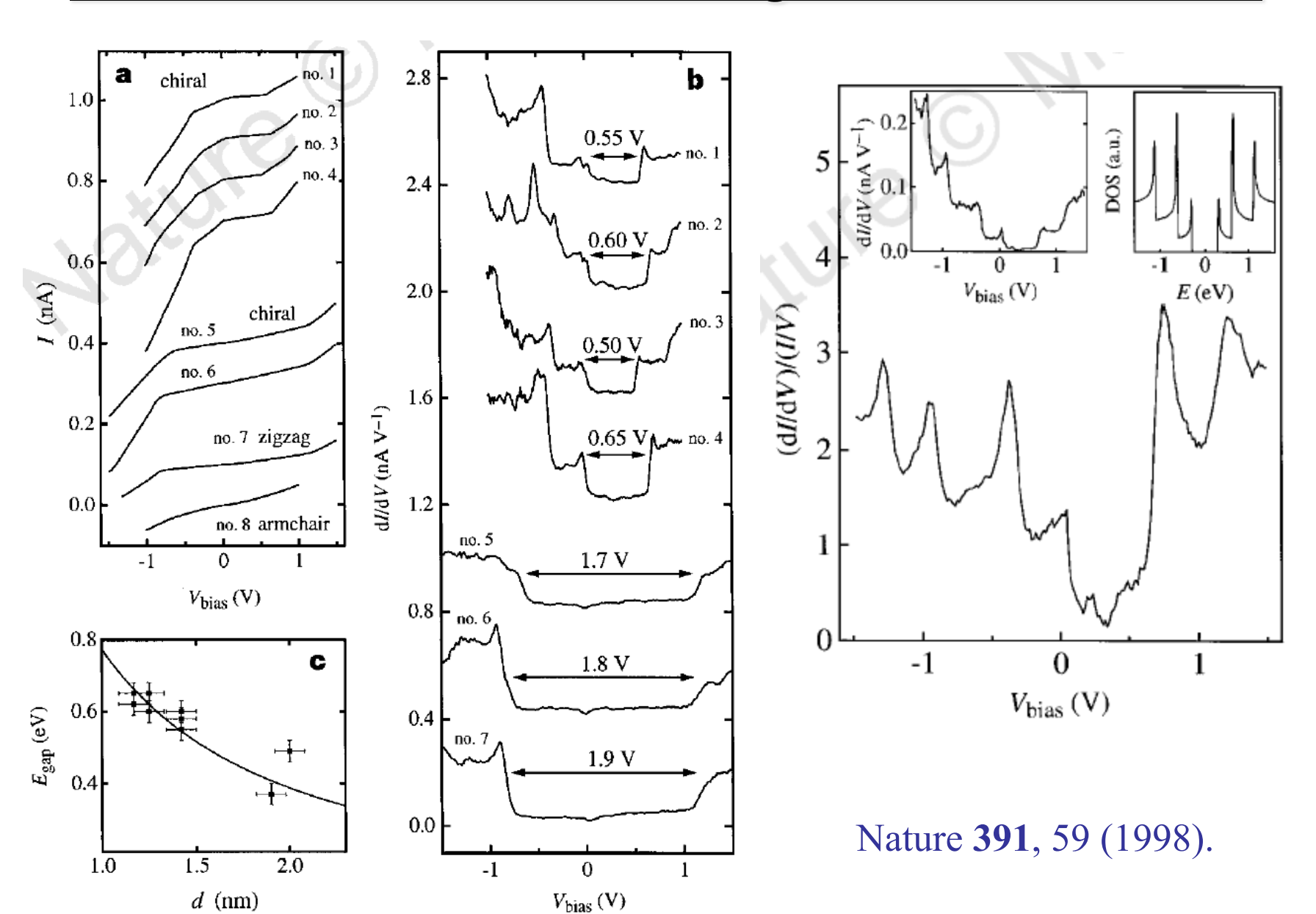


- 1. Science **234**, 304-309 (1986).
- 2. Phys. Rev. Lett. **56**, 1972-1975 (1986).

Density of states of various dimensions



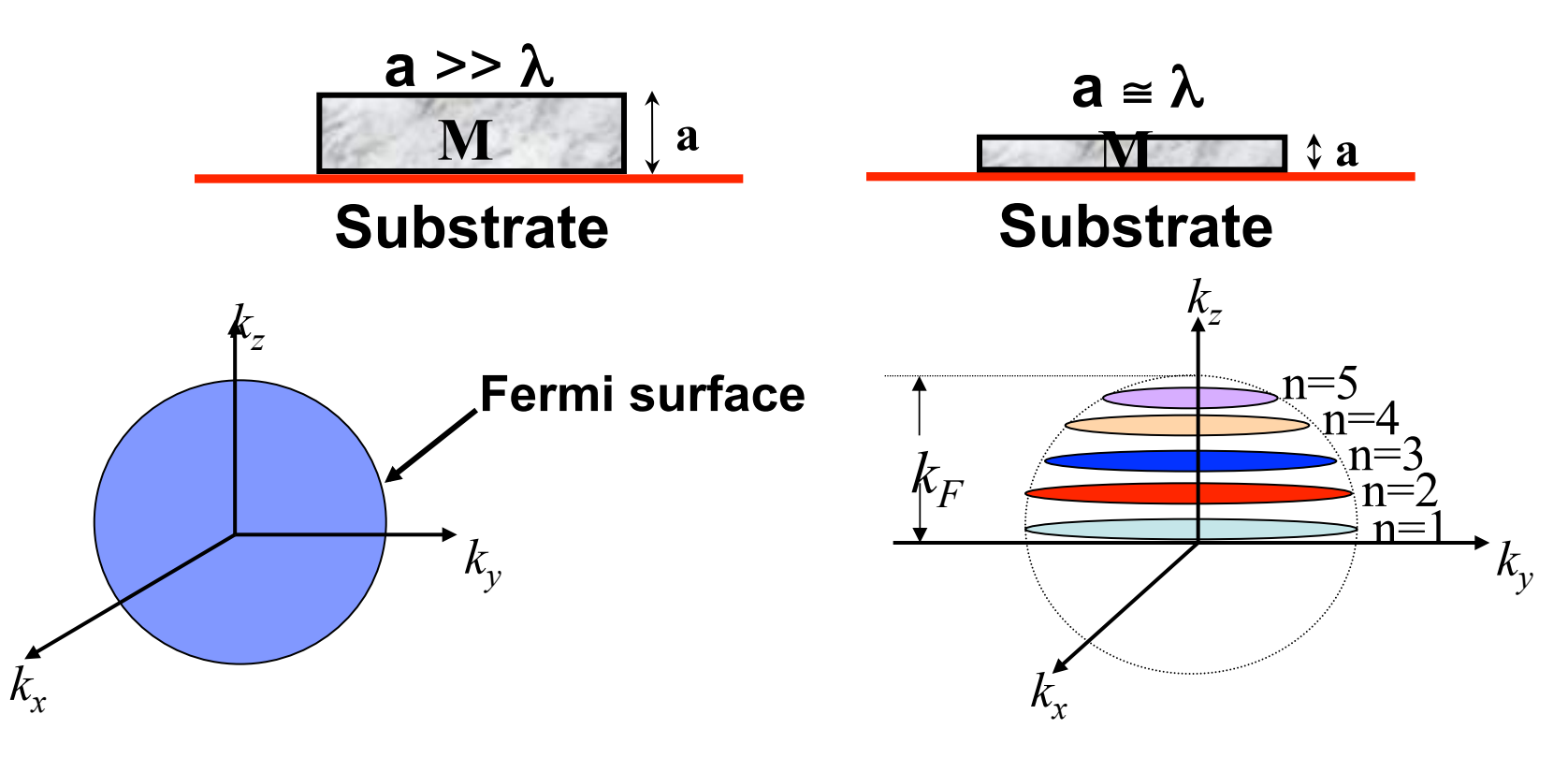
Electronic Structure of Single-wall Nanotubes



Quantum size effect

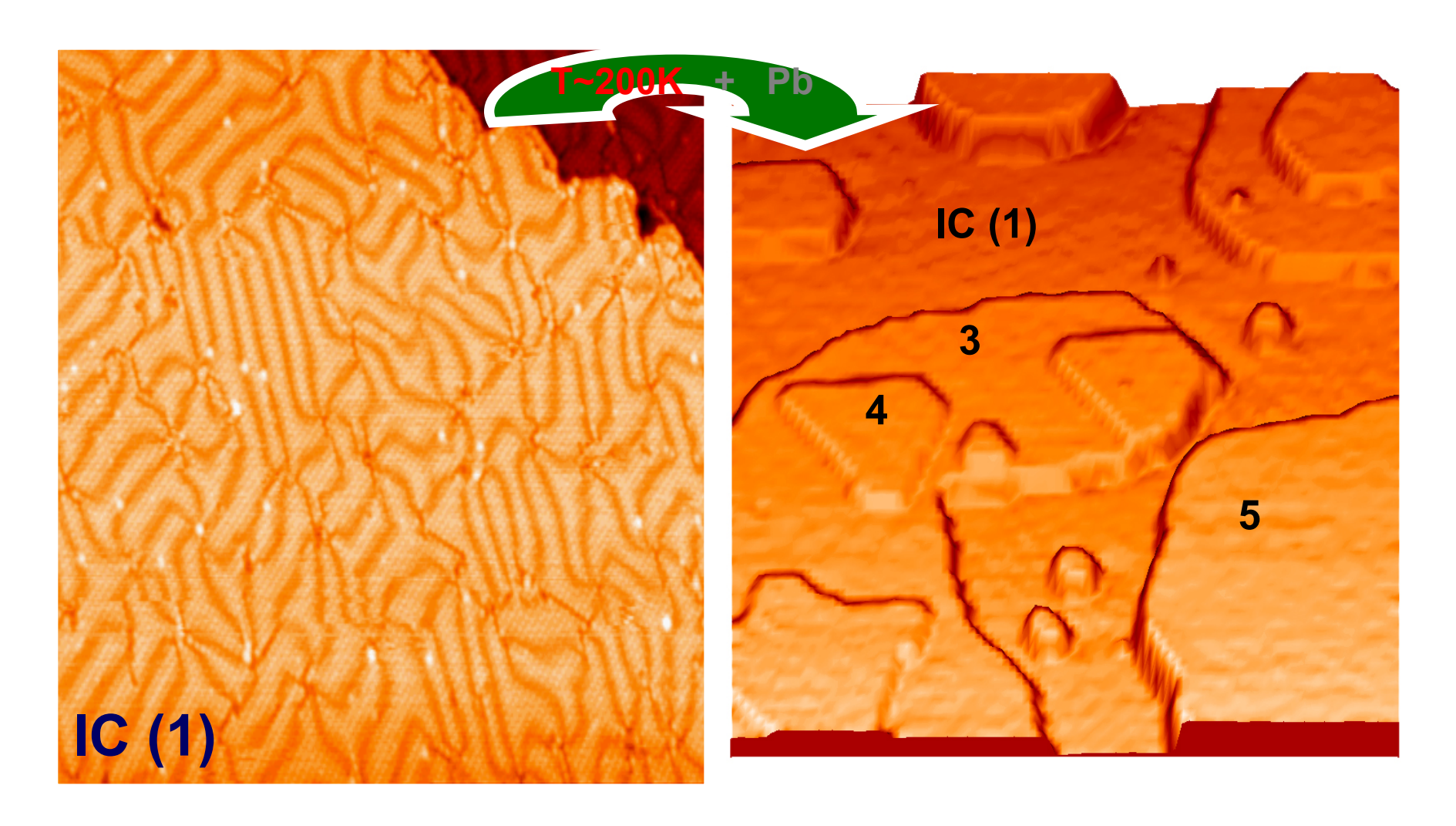
 λ = de Broglie wavelength of electron

a = thickness of metal film



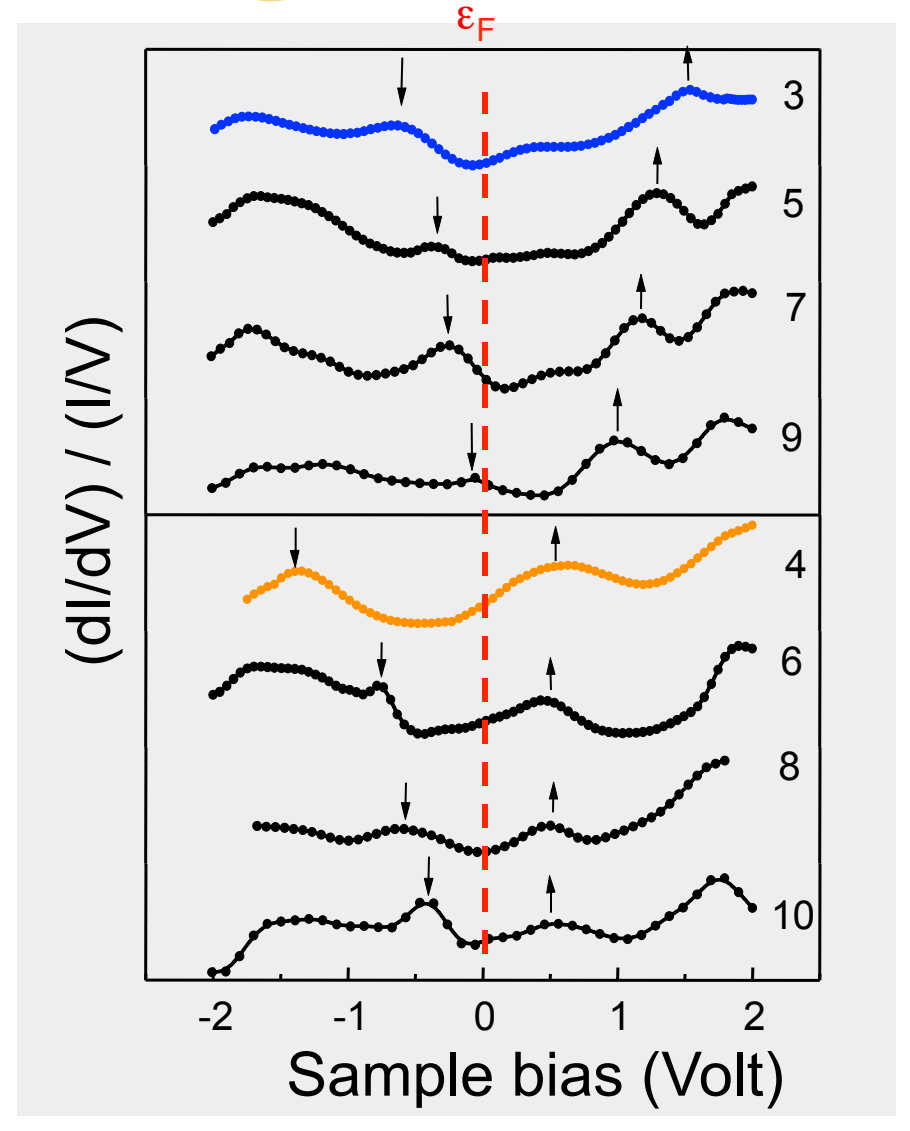


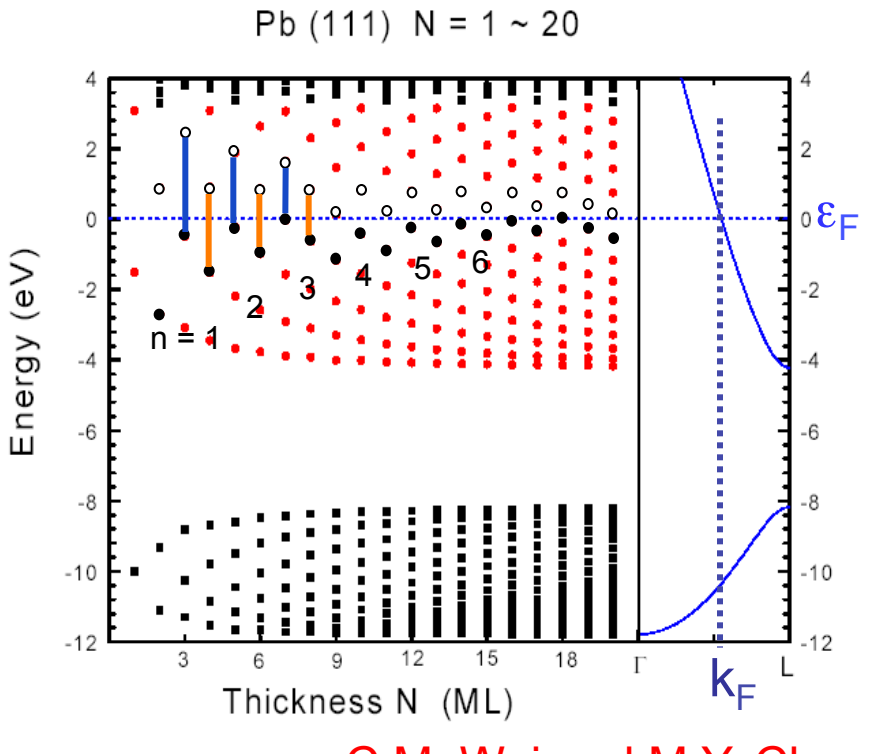
Pb islands on the IC Pb/Si(111)





Spectra for Pb Films



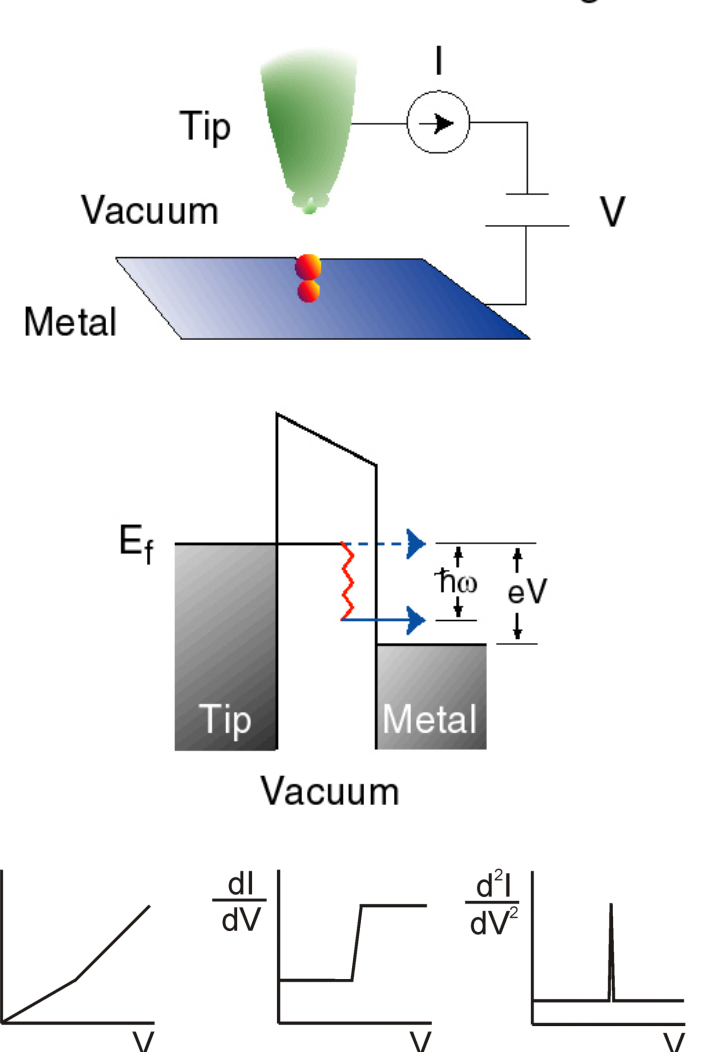


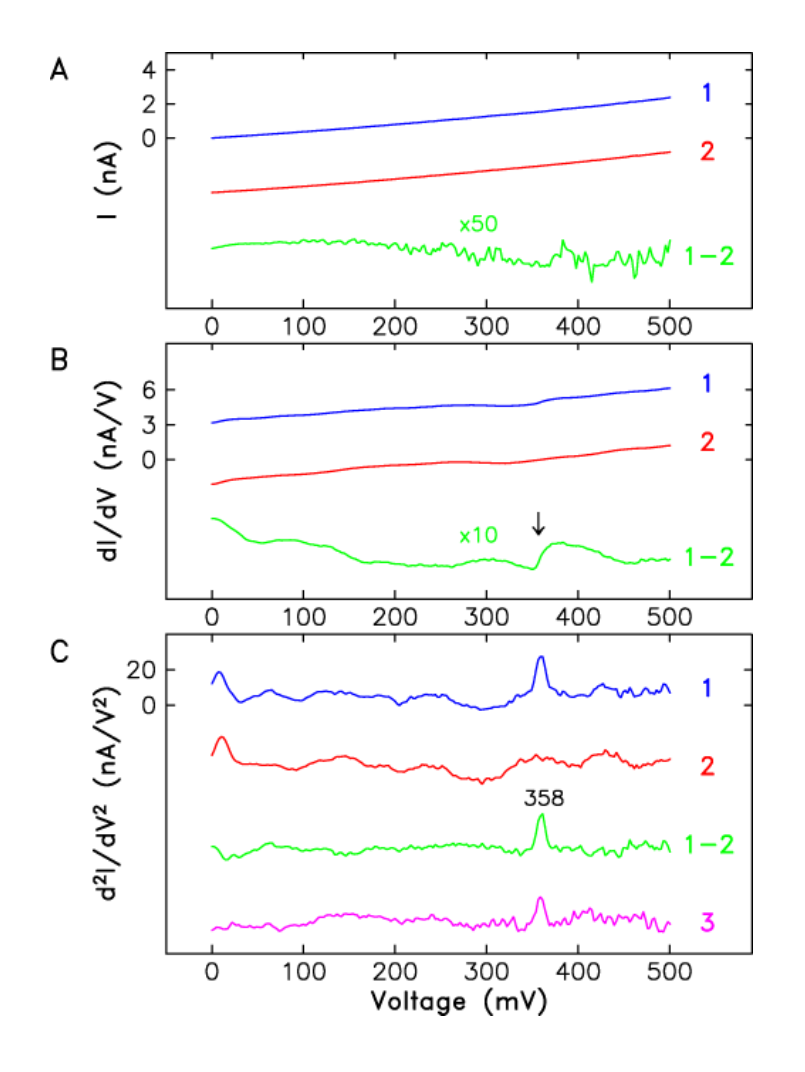
C.M. Wei and M.Y. Chou

$$d_0 = 2.85 \text{ Å}$$
 $\lambda_F = 3.94 \text{ Å}$ $2d_0 \approx 3(\lambda_F/2)$

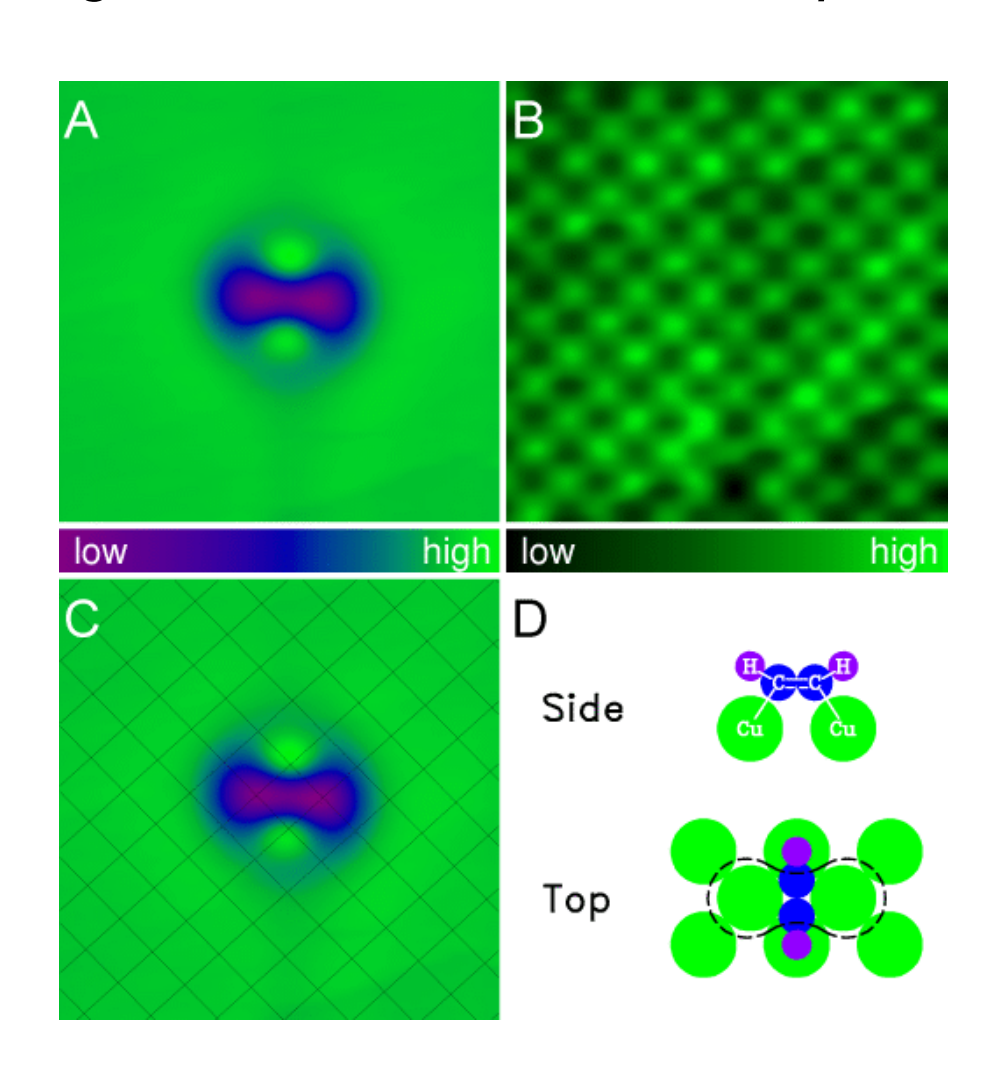
Inelastic Tunneling

Elastic vs. Inelastic Tunneling

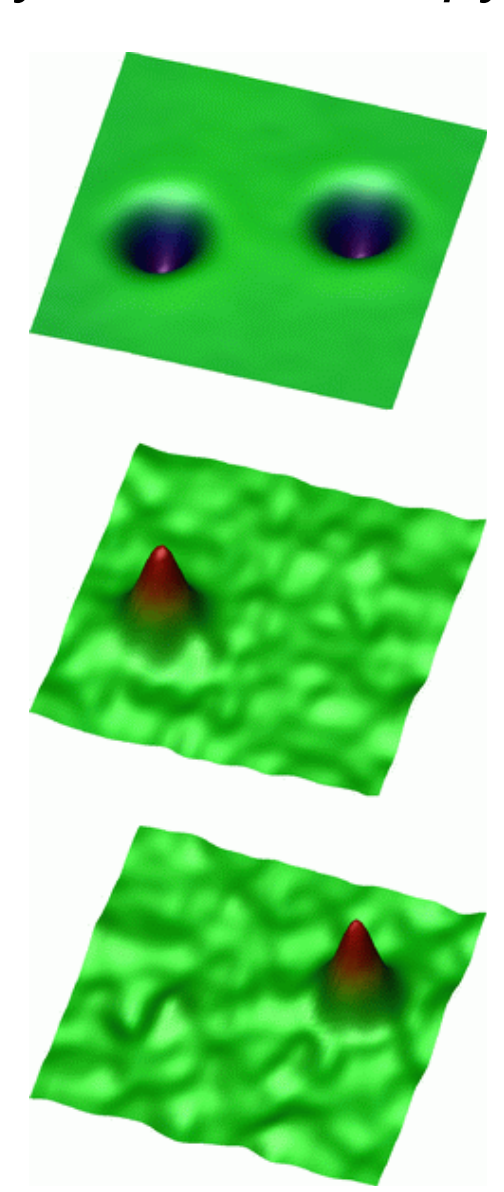




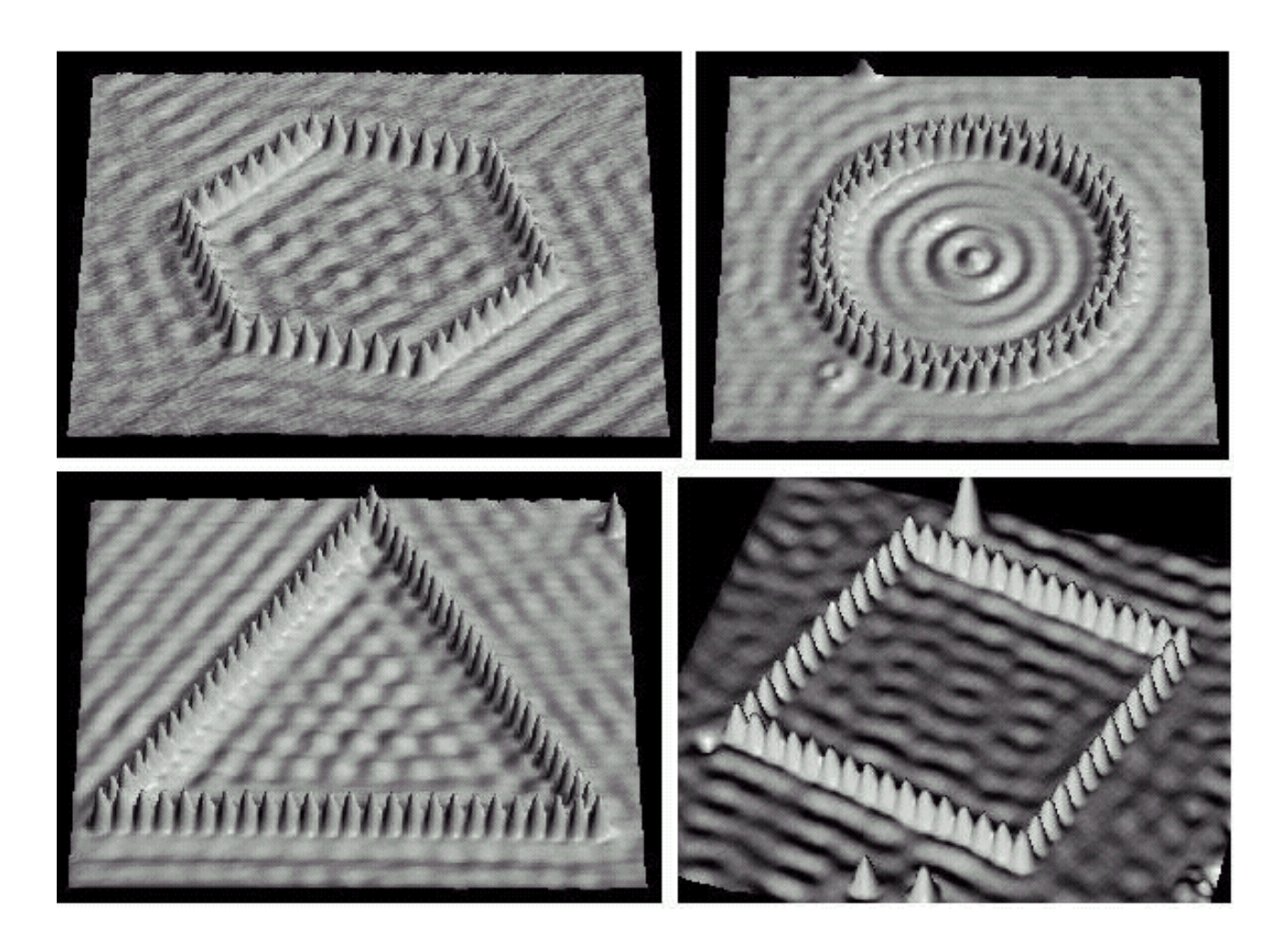
Single Molecule Vibrational Spectroscopy and Microscopy



B.C. Stipe, M.A. Rezaei, and W. Ho, Science **280**, 1732-1735 (1998).

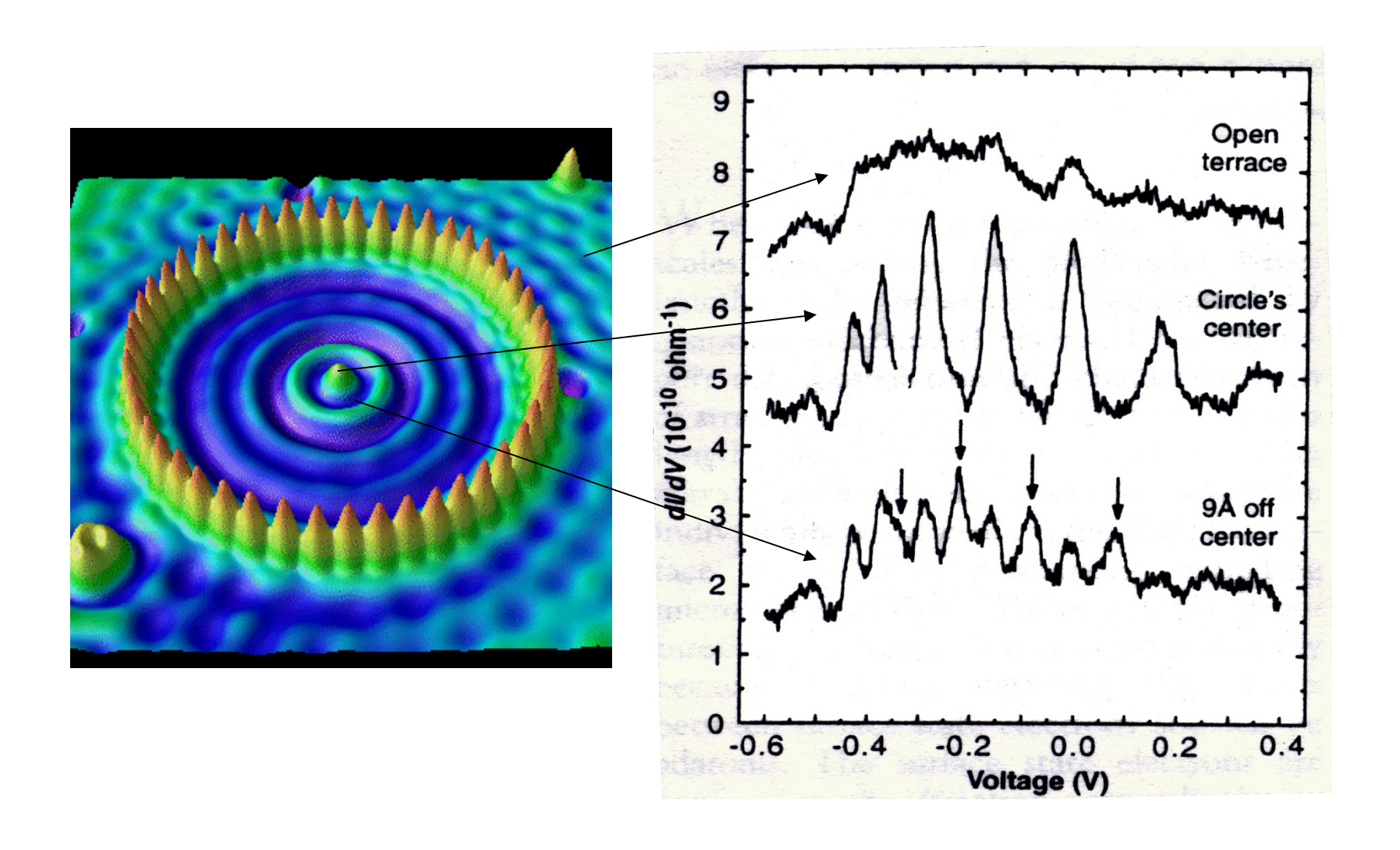


Quantum corral



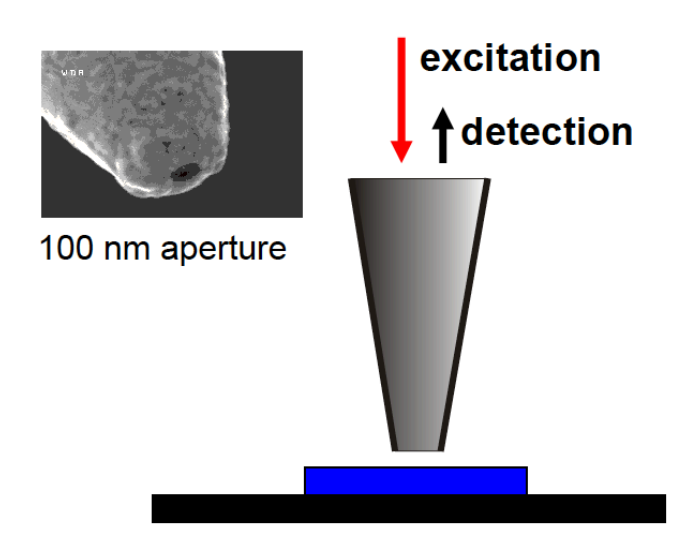
D.M. Eigler, IBM, Amaden

Artificial atom



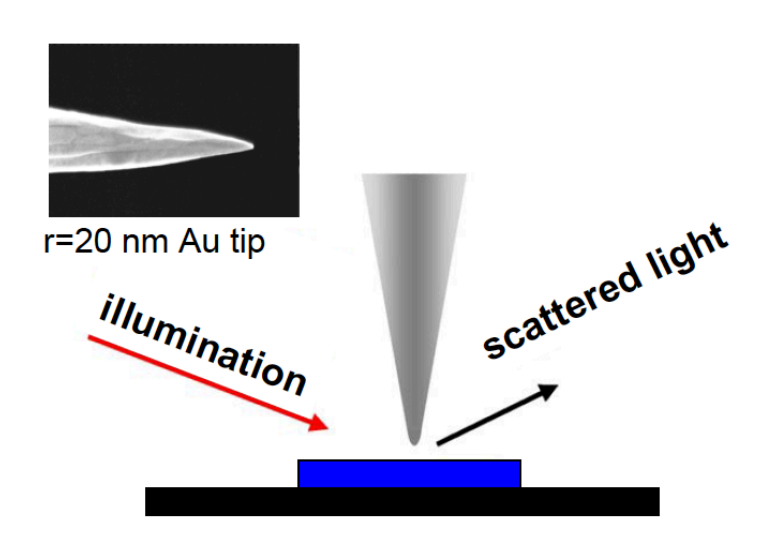
Optical methods with sub-wavelength spatial resolution

Aperture near-field probes



Spatial resolution 100 nm
Time resolution 100 fs - cw
Spectral resolution (cw) 30 µeV
Sample temperatures 10 - 300 K

Apertureless scattering

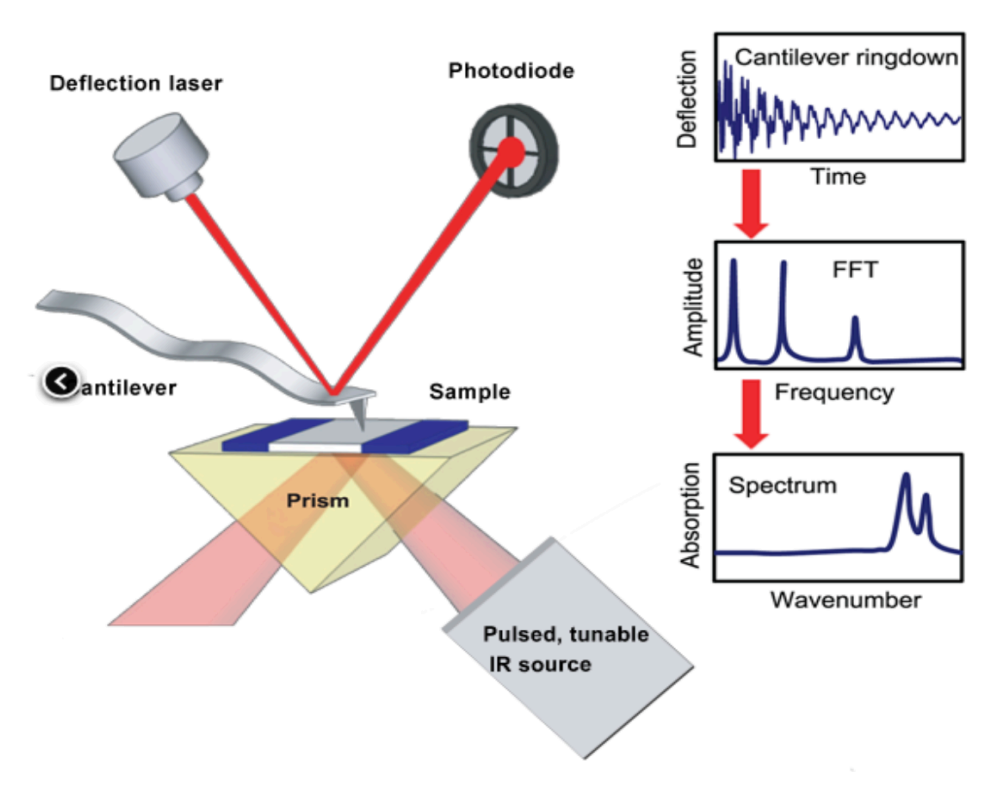


10 nm 10 fs - cw several meV

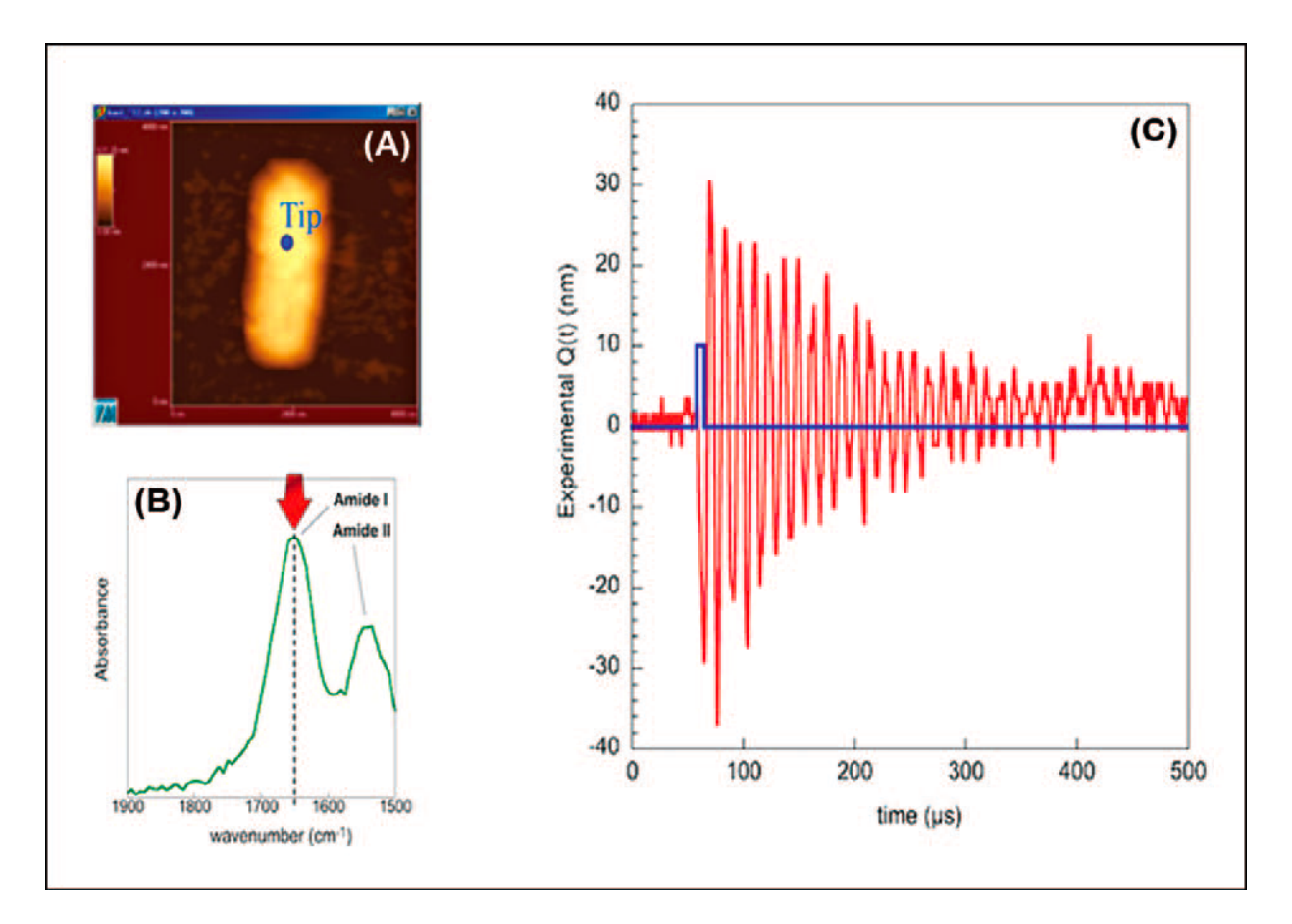
300 K

Recent development: AFM-IR system

AFM-IR can perform IR spectroscopic chemical identification with sub-100 nm spatial resolution



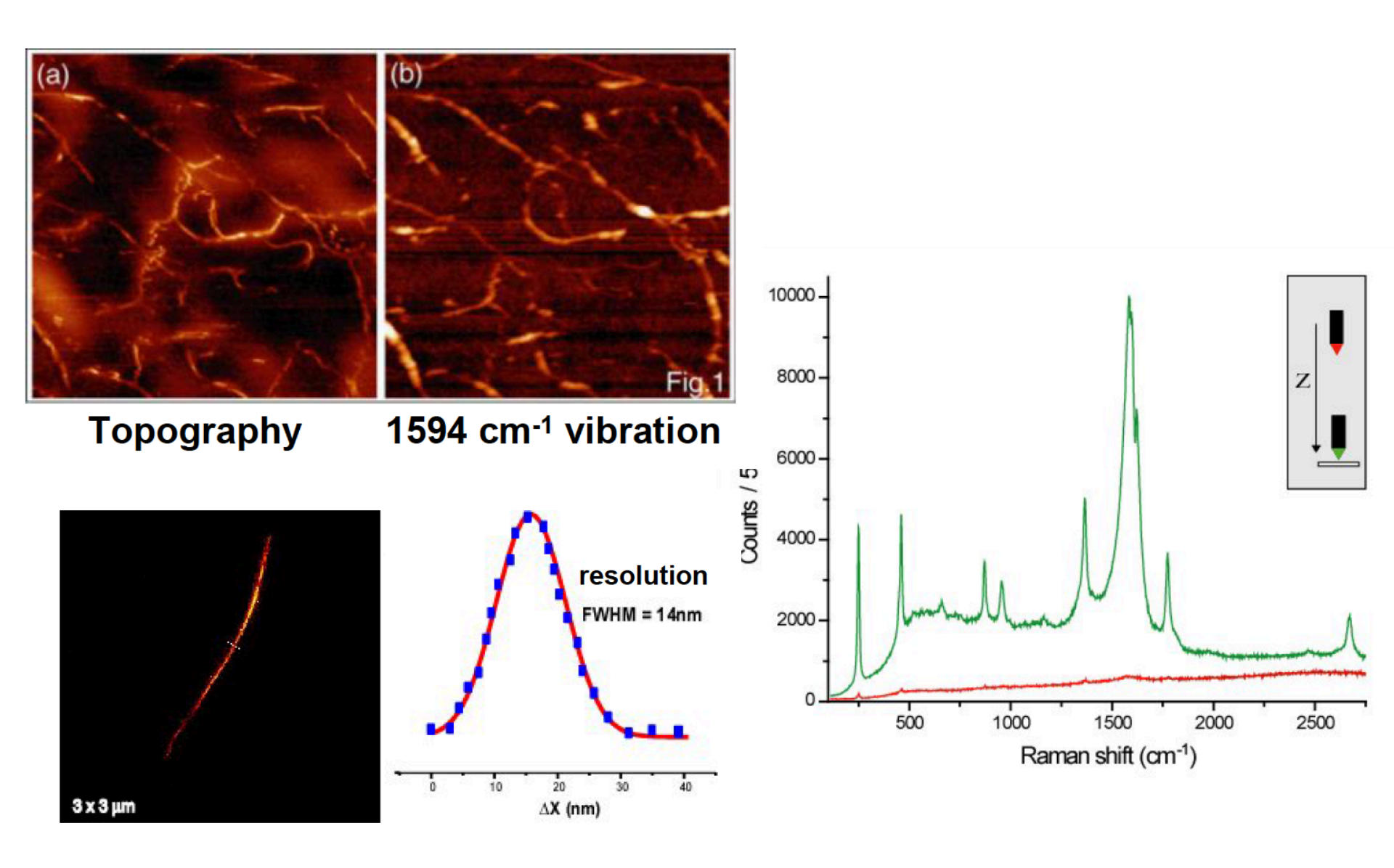
Scheme of the AFM–IR setup. The AFM cantilever ring-down amplitude plotted as a function of laser excitation wavelength produces the IR spectrum.



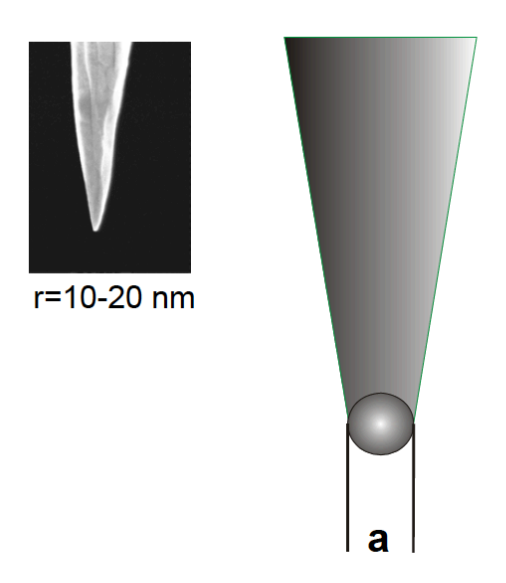
(a) AFM topography picture of the bacterium; the position of the tip is indicated in blue. (b) FT–IR spectrum; the bacterium absorption spectrum is drawn in green, and the wavenumber of the CLIO laser is indicated by the red arrow. (c) Oscillations recorded by the four-quadrant detector (in red) as function of time superposed on the CLIO pulse laser (blue).

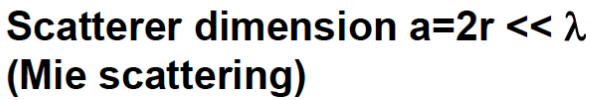
Alexandre Dazzi et al., APPLIED SPECTROSCOPY OA 66, 1365 (2012)

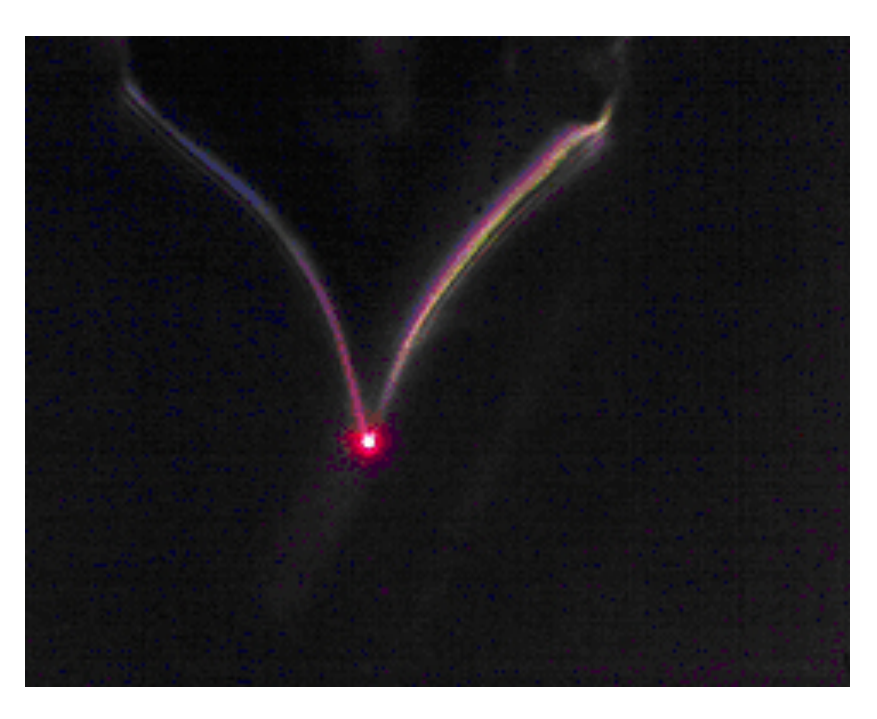
Tip-enhanced Raman spectroscopy



Light scattering from a metallic nanotip





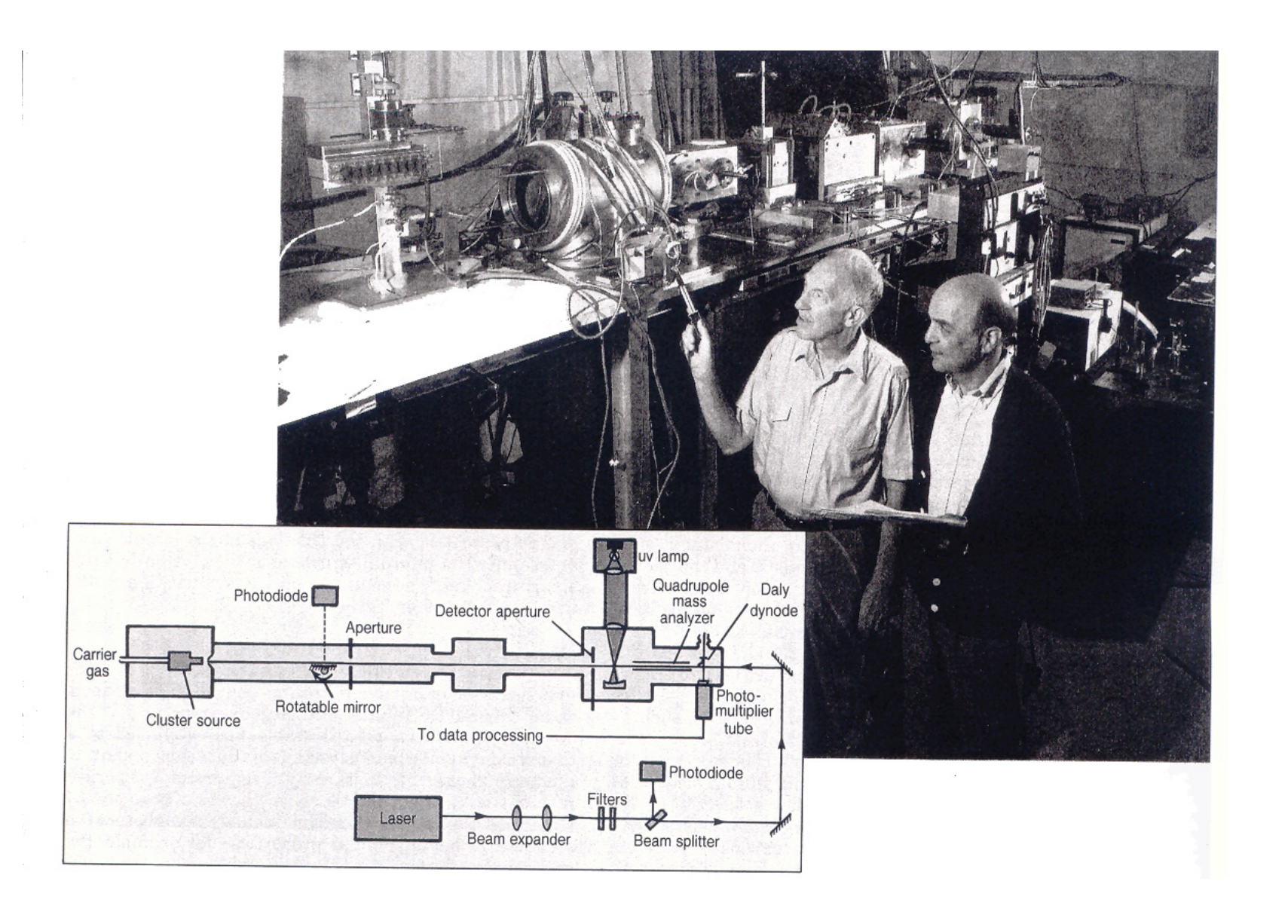


Electric field enhancement for field vector parallel to tip axis:

- lightning rod effect (field singularity at tip apex)
- surface plasmon excitation

Field enhancement factor 10 – 50

L. Novotny et al., Phys. Rev. Lett. 79, 645 (1997), Annu. Rev. Phys. Chem. 57, 303 (2006)



Mass Analyzer

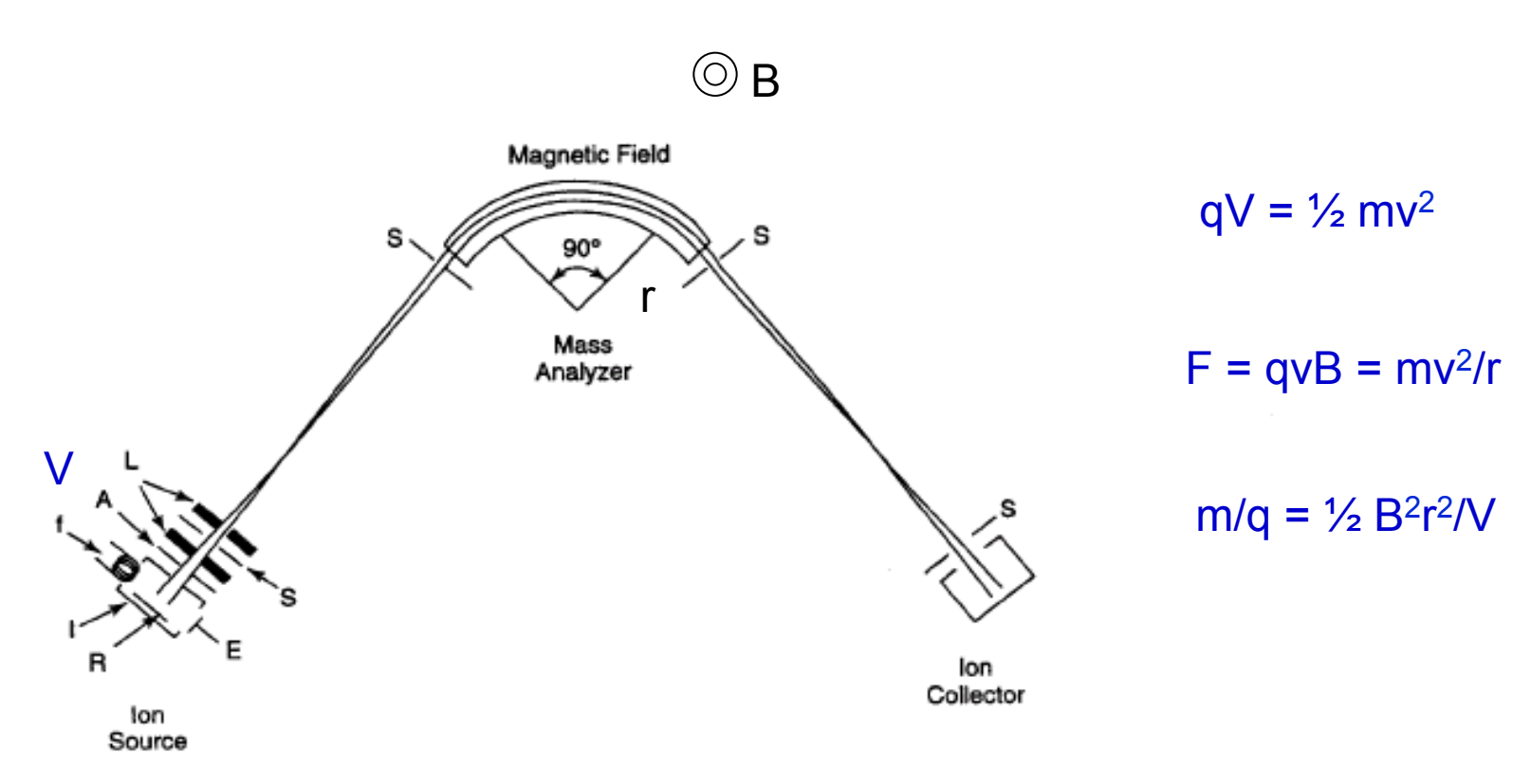
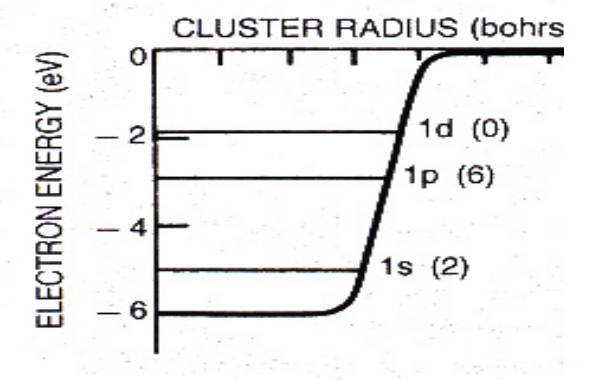
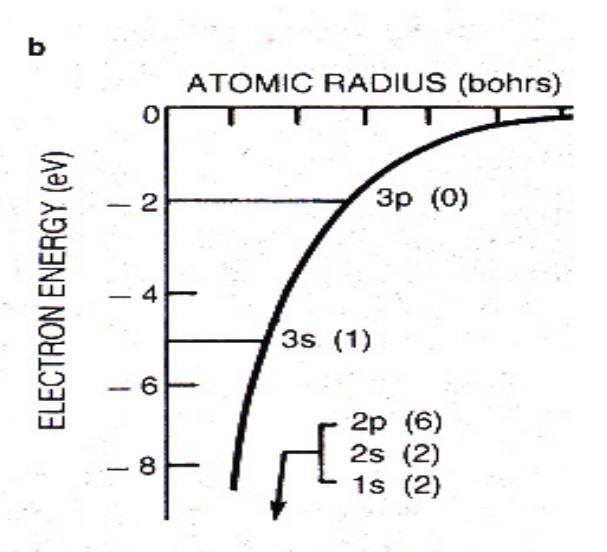


Figure 3.8. Sketch of a mass spectrometer utilizing a 90° magnetic field mass analyzer, showing details of the ion source: A—accelerator or extractor plate, E—electron trap, f—filament, I—ionization chamber, L—focusing lenses, R—repeller, S—slits. The magnetic field of the mass analyzer is perpendicular to the plane of the page.





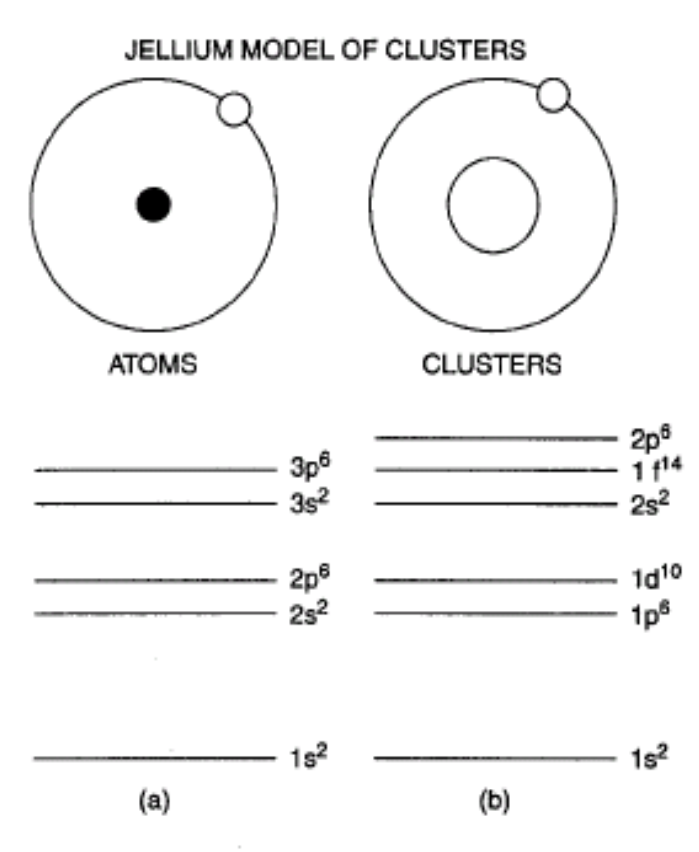
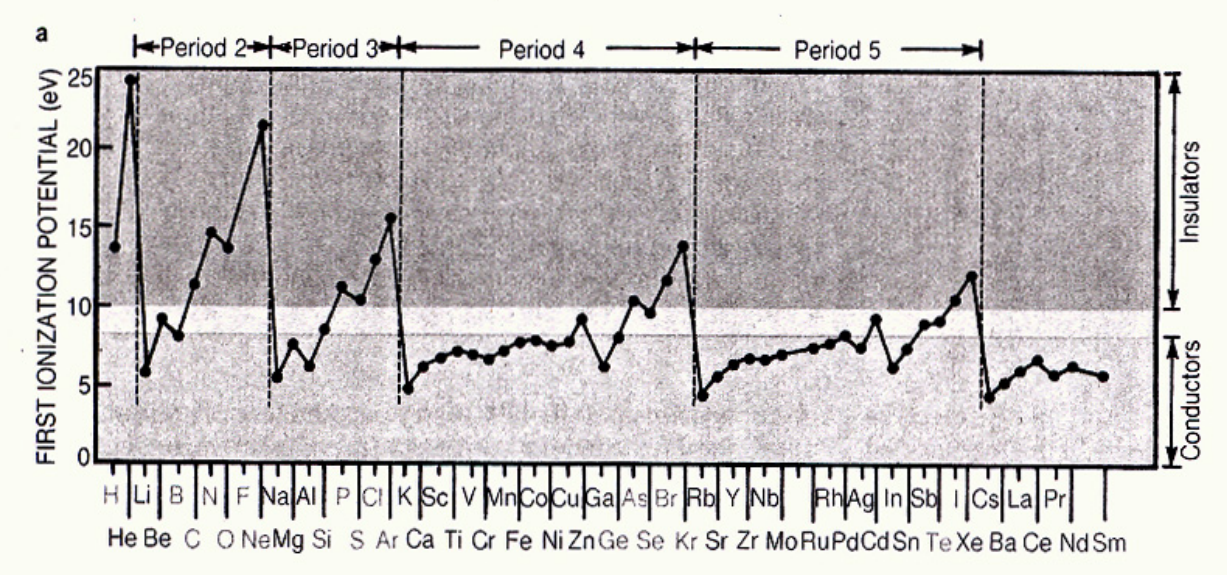
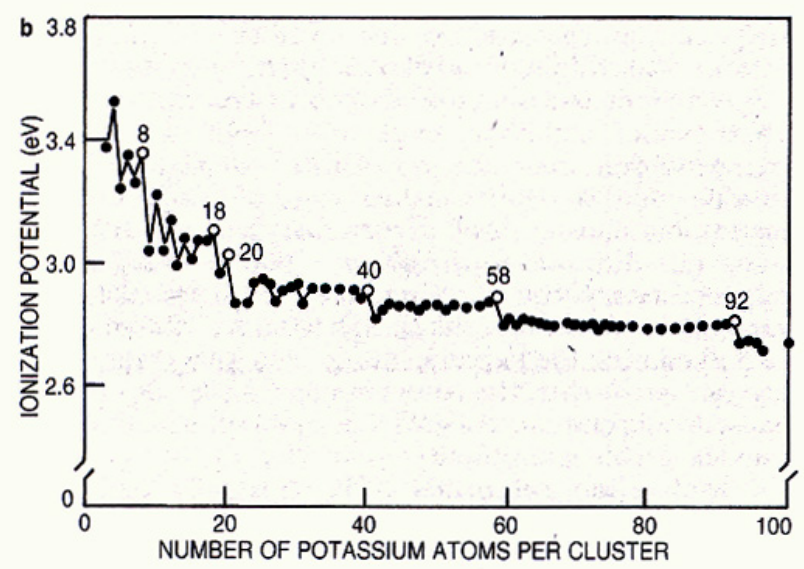
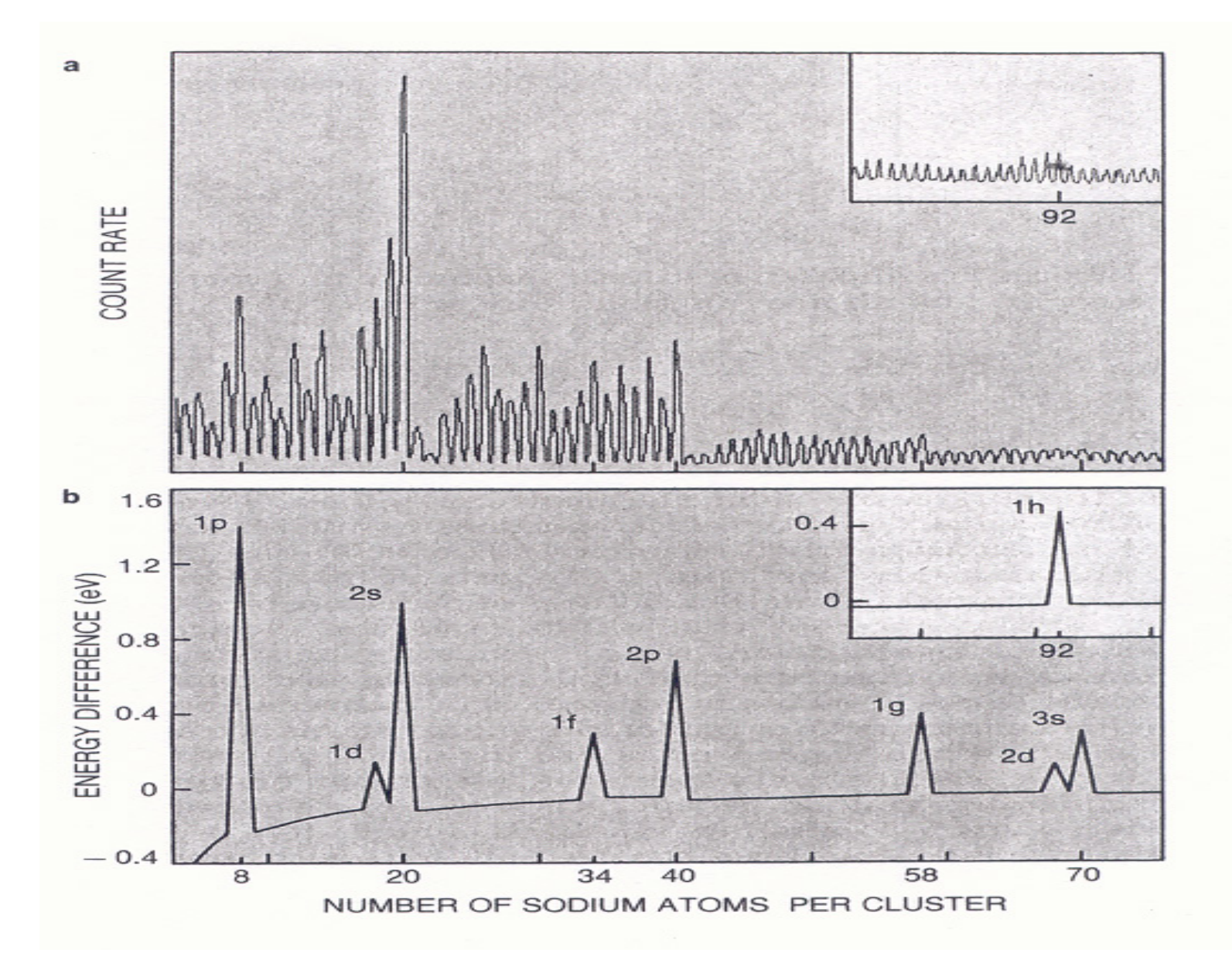


Figure 4.5. A comparison of the energy levels of the hydrogen atom and those of the jellium model of a cluster. The electronic magic numbers of the atoms are 2, 10, 18, and 36 for He, Ne, Ar, and Kr, respectively (the Kr energy levels are not shown on the figure) and 2, 18, and 40 for the clusters. [Adapted from B. K. Rao et al., *J. Cluster Sci.* **10**, 477 (1999).]





Shell structure: Two views. a: Atomic ionization potentials drop abruptly from above 10 eV following the shell closings for the noble gases (He, Ne, Ar and so on). For semiconductors (labeled in blue) the ionization potential is between 8 and 10 eV, while for conductors (red) it is less than 8 eV. It is clear that bulk properties follow from the natures of the corresponding atoms. (Adapted from A. Holden, The Nature of Solids, © Columbia U. P., New York, 1965. Reprinted by permission.) b: Ionization potentials for clusters of 3 to 100 potassium atoms show behavior analogous to that seen for atoms. The cluster ionization potential drops abruptly following spherical shell closings at N = 8, 20, 40 Features at N = 26 and 30 represent spheroidal subshell closings. The work function for bulk potassium metal is 2.4 eV. Figure 3



Reactivity of nanoclusters

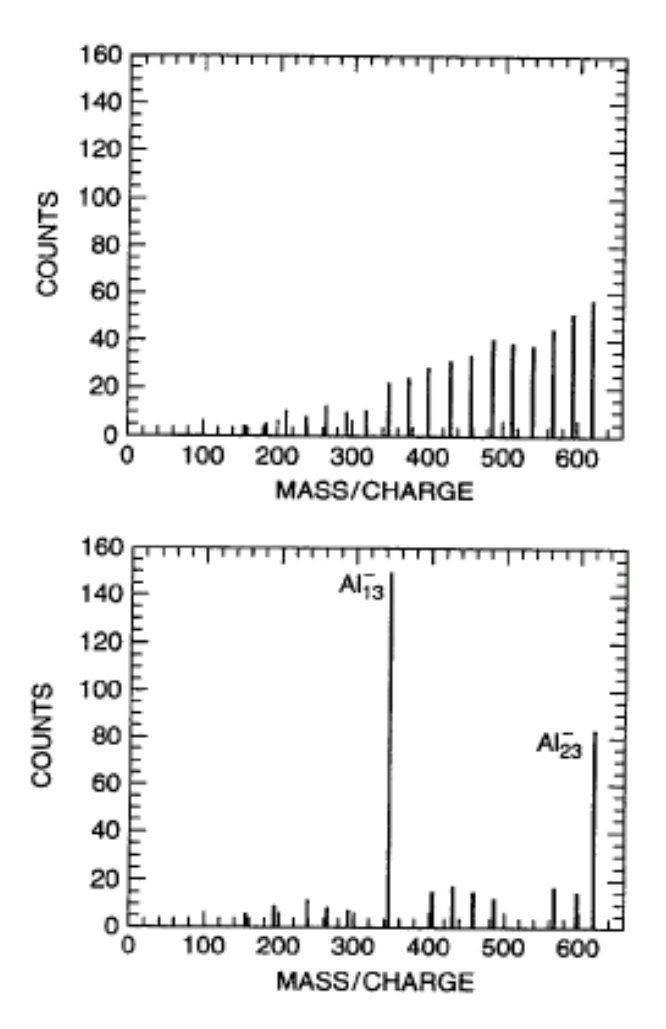


Figure 4.13. Mass spectrum of Al nanoparticles before (top) and after (bottom) exposure to oxygen gas. [Adapted from R. E. Leuchtner et al., J. Chem. Phys., 91, 2753 (1989).]

Magic clusters

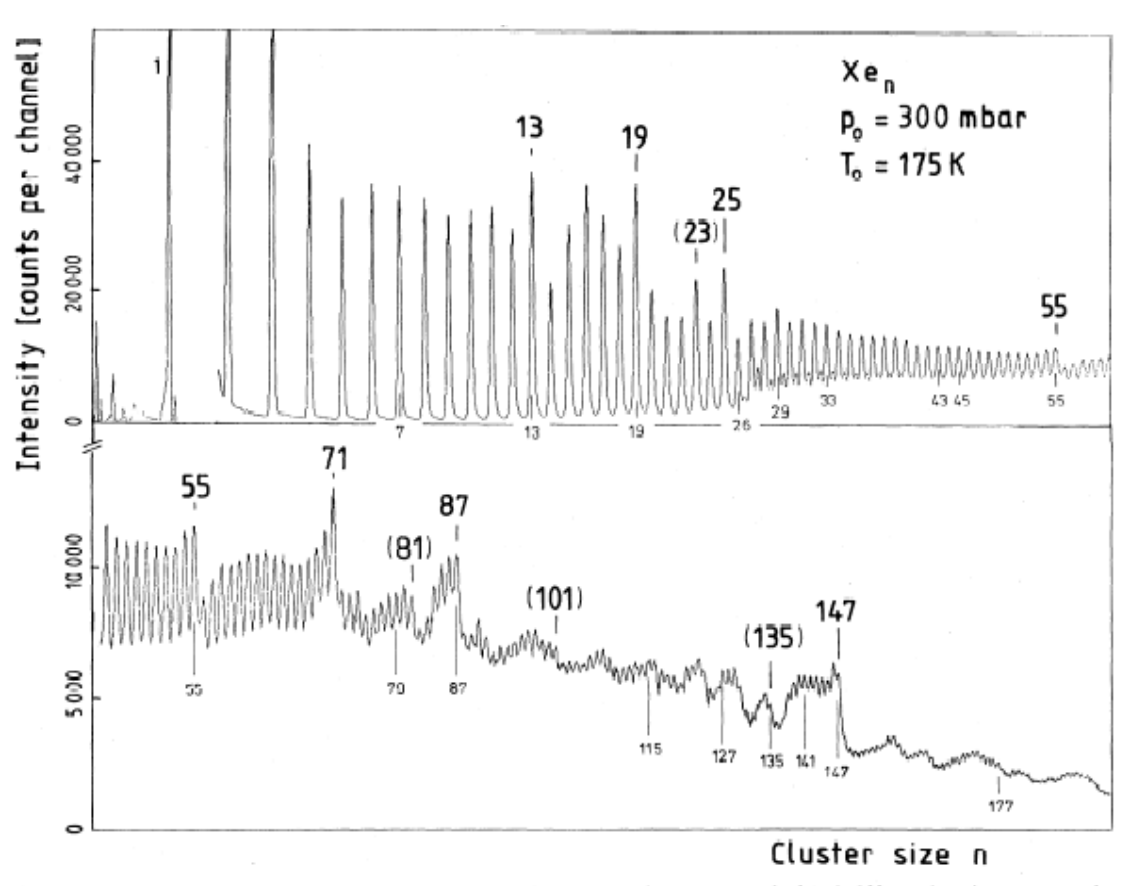
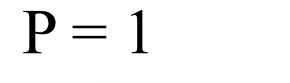


FIG. 1. Mass spectrum of kenon clusters. Observed magic numbers are marked in boldface; brackets are used for numbers with less pronounced effects. Numbers below the curve indicate predictions or distinguished sphere packings.

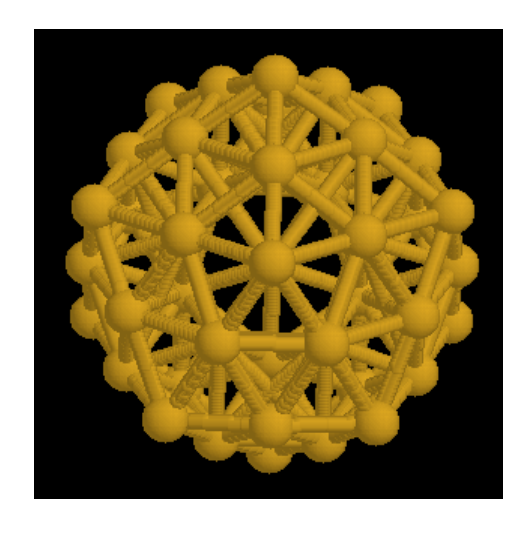
Mackay icosahedra



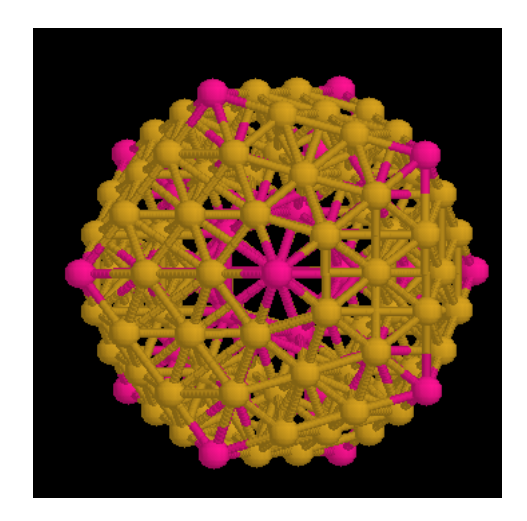


20 fcc(111) faces

P = 2



P=3



Shell model

$$N = 1 + \Sigma (10p^2 + 2)$$

